RESULTS

Expression of CD3ε and FcγRIIB in the developing cerebellum. We examined the distributions of CD3ε and FcγRIIB proteins in the mouse cerebellum at P21 by double immunofluorescence using cellular and subcellular markers. CD3ε and FcγRIIB proteins were distributed widely in the cerebellar cortex (Fig. 1). The most intense staining of CD3ε and FcγRIIB was found in perikarya and dendritic shafts of PCs, because each immunostaining showed considerable overlap with Car8 (Fig. 1A and B), a molecule known to be exclusive in PCs and responsible for ataxic mutant Waddles mice (11, 12). At a higher magnification, CD3ε and FcγRIIB were also detected in Car8-labeled dendritic spines of PCs (Fig. 1A, lower panels). Outside Car8-labeled PC elements, CD3ε and FcγRIIB were also distributed at low to moderate levels. To address these cellular elements, we used VGLUT1 and GLAST as a marker for parallel fiber terminals and Bergmann glia, respectively. Little, if any, CD3ε and FcγRIIB were detected in VGLUT1-labeled parallel fiber terminals (Fig. 1C), whereas they were found in GLAST-positive cell bodies and processes of Bergmann glia (Fig. 1D). A slight difference was also found in that CD3ε was detected in both Bergmann fibers (i.e., rod-like staining) (Fig. 1D) and lamellate processes (reticular staining in the neuropil), while FcγRIIB was preferentially seen in lamellate processes. Therefore, CD3ε and FcγRIIB are coexpressed in PCs and Bergmann glia in the cerebellar cortex.

Impaired cerebellar architecture in both CD3ε-deficient and FcγRIIB-deficient mice during development. In T cells, all CD3 subunits are assembled in the TCR-CD3 complex. The current model of TCR-CD3 signaling in T cells assumes coordinated regulation by all CD3 subunits. Phosphorylation of the ITAMs in CD3ζ is a critical step for actin polymerization, whereas the remaining CD3 subunits also participate in the signaling (5, 13). Therefore, we examined if the CD3 signaling machinery is established in the cerebellum. CD3γ and CD3δ transcripts were also found in the cerebellum at developmental stages. In contrast, CD3ζ mRNA was not detected at any stages of development using two sets of CD3ζ-specific primers (Fig. 2A), indicating that CD3 signaling components, such as CD3ε, CD3γ, and CD3δ, exist in the cerebellum, whereas the CD3 signaling seems to differ in the cerebellum from that in the immune system. Furthermore, CD3ε was preferentially expressed in the developmental stages. The CD3ε mRNA level was highest at P21. Therefore, we asked whether CD3ε and FcγRIIB contribute to the formation of neuronal architecture during development. We used two mutant mice, FcγRIIB-deficient mice and CD3ε-deficient mice, in which CD3δ is also not detected and the CD3γ protein level is reduced (16).

In the control mice, migrating NeuN-positive GCs with an ellipsoidal shape were observed at P7, whereas in the two mutant mice, these cells were round (Fig. 2B). Furthermore, when we quantified the area filled by GCs in IGL, a reduction was observed in the two knockout mice at both P3 and P7 (Fig. 2C). We then examined the development of PC dendrites. At P7, the size of the dendritic arbor and degree of branching of PCs were reduced in the two knockout mice compared to the control mice, as verified by calbindin staining (Fig. 2D). GCs extend PFs, and as the PFs extend, they make synaptic contact

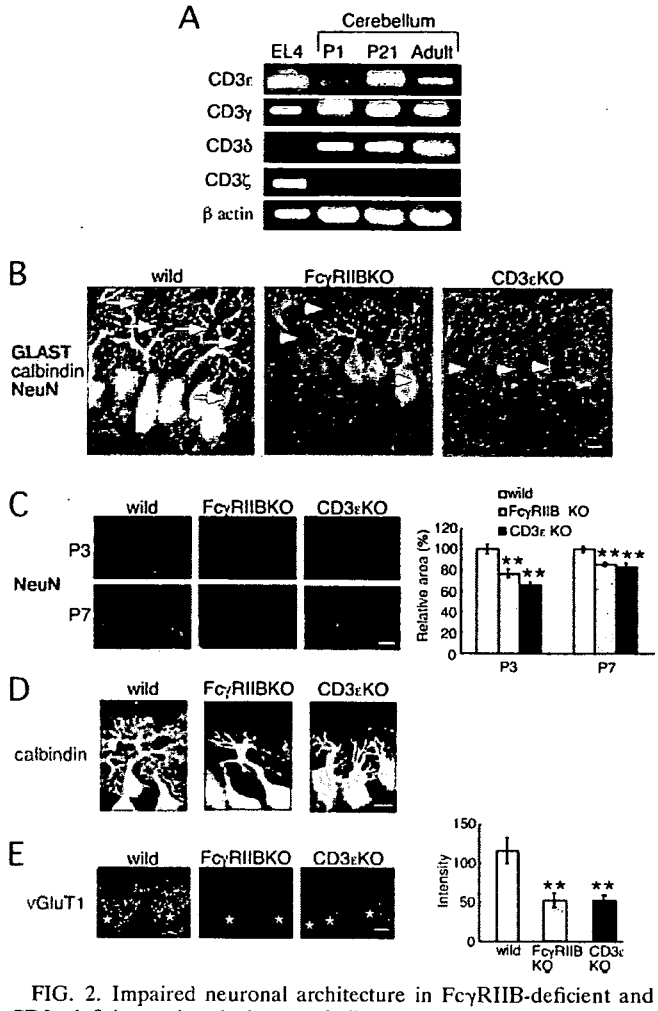

FIG. 2. Impaired neuronal architecture in FcγRIIB-deficient and CD3ε-deficient mice during cerebellar development. (A) RT-PCR analysis of each CD3 subunit in the EL4 T-cell line and the cerebellum from C57BL/6 mice at P1, P21, and the adult stage. β-Actin was used as the internal control. (B) Triple immunofluorescence for GLAST (red), calbindin (green), and NeuN (blue) at P7. Arrows and arrowheads indicate migrating GCs with an ellipsoidal shape and those with a round shape, respectively. (C) Immunofluorescence for NeuN at P3 and P7. The relative area occupied by granule cells was quantitatively compared. (D) Immunofluorescence for calbindin at P7. (E) The pixel intensity of VGLUT1 immunofluorescence was quantitatively compared. The left panel shows representative examples of immunofluorescence staining with anti-vGluT1 antibody at P7. The images were taken at the same exposure. Asterisks, Purkinje cell somata. Bars, 10 μm.

with the forming PC dendritic arbors. Synaptic terminals of PFs can be detected with anti-VGLUT1 antibody. In both mutant mice, the intensity of VGLUT1 signal was reduced at P7 (Fig. 2E).

CD3 and FcγRIIB have a common role in PF-PC synaptic function. Given the impaired development of PCs in the two mutant mice, we investigated whether these two molecules have common roles in synaptic functions in the adult by using electrophysiological approaches. We examined EPSCs in response to the stimulation of PFs or CFs in 8- to 10-week slice preparations by whole-cell patch clamping. There was no statistically significant difference in passive membrane properties between wild-type and FcγRIIB-deficient PCs (data not

TABLE 1. Basic properties of CF and PF EPSCs[a]

Synapse type	10–90% rise time[b] (ms)			Decay time constant[c] (ms)		
	Wild type	FcγRIIB KO	CD3ε KO	Wild type	FcγRIIB KO	CD3ε KO
CF EPSC	0.5 ± 0.1 (12)	0.5 ± 0.1 (15)	0.5 ± 0.1 (11)	14.1 ± 3.2 (12)	13.5 ± 3.6 (15)	12.7 ± 3.9 (11)
PF EPSC	2.7 ± 0.6 (15)	2.8 ± 0.7 (15)	2.7 ± 0.7 (15)	22.1 ± 5.5 (15)	22.5 ± 6.2 (15)	23.4 ± 5.7 (15)

[a] Data represent means ± standard deviations; *n* is reported in parentheses. KO, knockout.
[b] The time required for the synaptic current to increase from 10% to 90%.
[c] Current decay was fitted to single exponential curves.

shown). Basal transmission at PF-PC and CF-PC synapses was not significantly altered; there was no significant difference in either the rise or decay time constants of EPSCs between wild-type and FcγRIIB-deficient mice (Table 1). To investigate short-term synaptic plasticity, PPF at PF-PC synapses and paired-pulse depression (PPD) at CF-PC synapses were investigated by administering pairs of PF or CF stimuli at different interstimulus intervals. The PPF ratio was significantly increased in FcγRIIB-null slices when the interpulse interval was 20 to 220 ms: the PPF ratio at an interpulse interval of 20 ms was 205 ± 10% (mean ± standard error of the mean [SEM]) in wild-type mice and 259 ± 11% in FcγRIIB-deficient mice (Fig. 3A). In contrast, the PPD ratio was not significantly changed in FcγRIIB-deficient mice at interpulse intervals ranging from 20 to 3,000 ms (Fig. 3B).

Immature PCs are innervated by multiple CFs that originate from the inferior olive of the medulla (4). As animals grow, redundant CFs are gradually eliminated. FcγRIIB-deficient mice had almost the same percentage (more than 90%) of PCs innervated with a single CF as the wild-type mice (Fig. 3C),

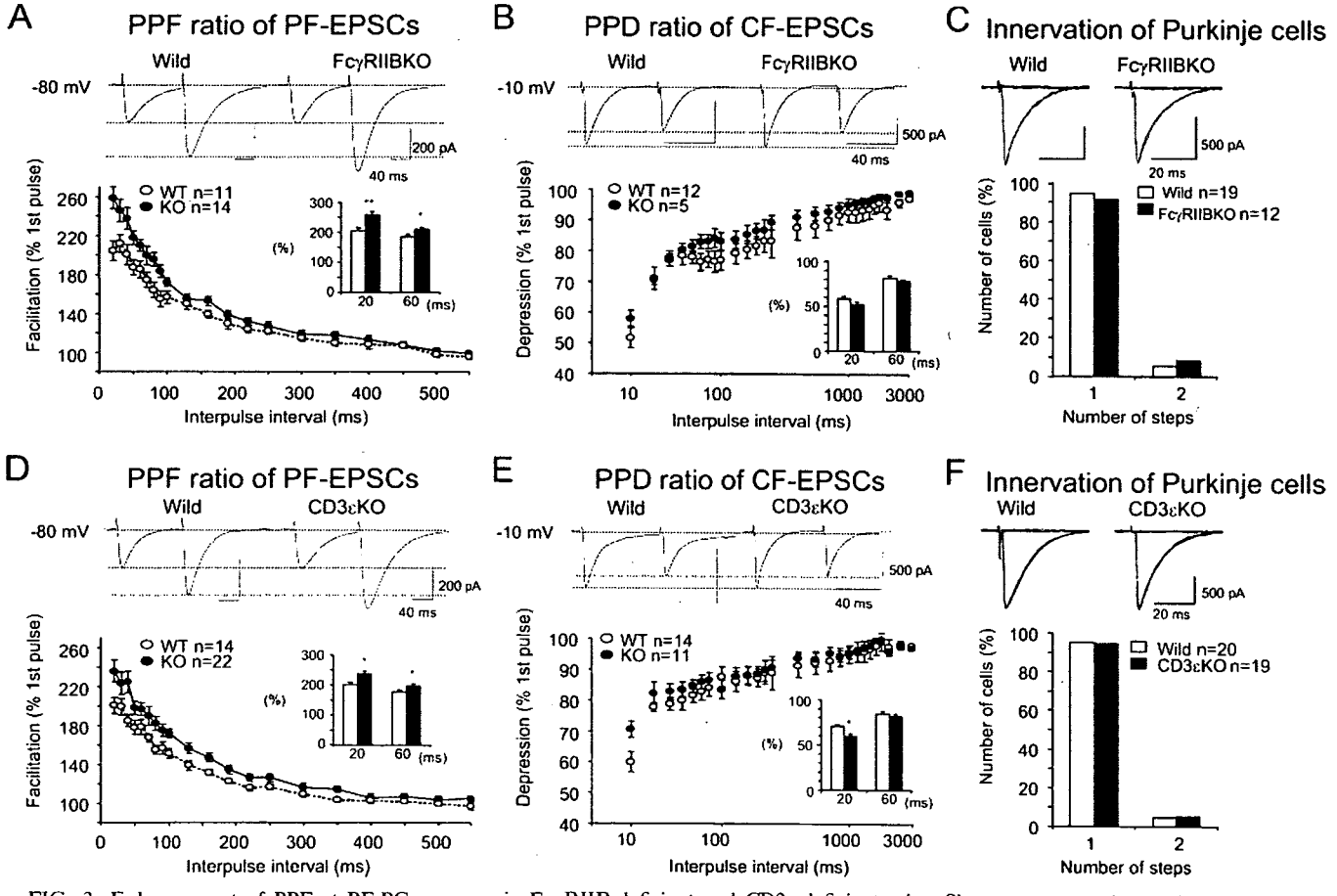

FIG. 3. Enhancement of PPF at PF-PC synapses in FcγRIIB-deficient and CD3ε-deficient mice. Short-term synaptic plasticity at PF- and CF-PC synapses was examined by applying pairs of stimuli separated by 20 to 550 ms or 20 to 3,000 ms. The second response (expressed as a percentage of the response to the first pulse; mean ± SEM) is plotted as a function of the interpulse interval. (A and D) PPF ratios of PF-EPSCs in FcγRIIB-deficient (A) and CD3ε-deficient (D) PCs were calculated. PF-EPSCs were obtained by holding membrane potentials at −80 mV. (B and E) PPD ratios of CF-EPSCs in FcγRIIB-deficient (B) and CD3ε-deficient (E) mice. (C and F) Single innervation of PCs by CFs in 8- to 10-week-old FcγRIIB-deficient (C) and CD3ε-deficient (F) mice. With gradually increasing stimulus intensities applied to the CFs, more than 90% of EPSCs of the wild-type and mutant mice were obtained in an all-or-none fashion. CF-EPSCs were elicited at −10 mV to inactivate voltage-dependent channels. Numbers of tested PCs (*n*) are indicated in each graph. *, $P < 0.05$.

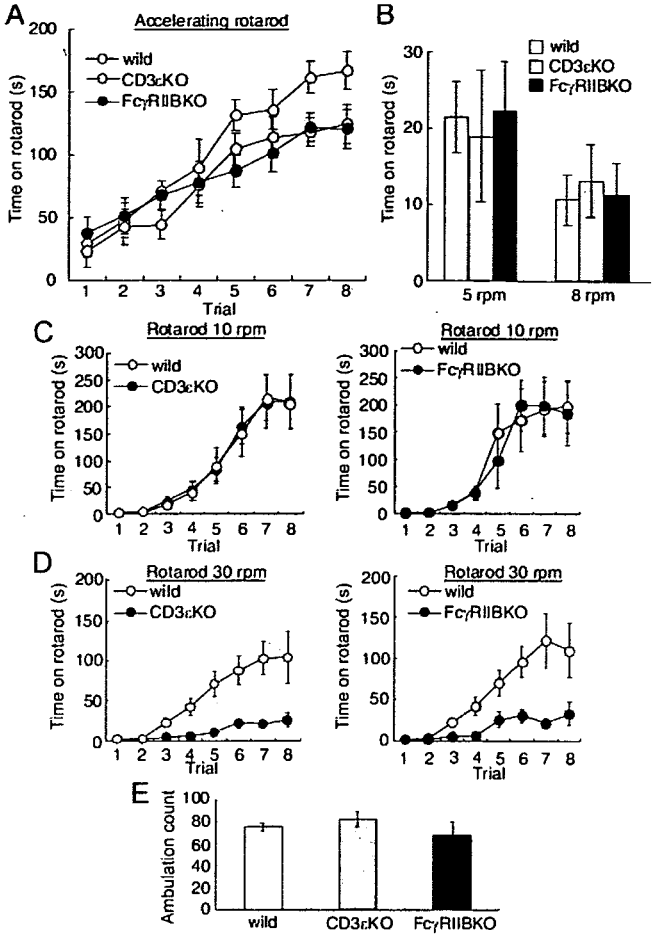

FIG. 4. Poor rotarod performance in FcγRIIB-deficient and CD3ε-deficient mice at high speed. (A) Amount of time mice remained on an accelerating rotarod over eight trials (n = 8 in each). (B) Amount of time mice remained on the rotarod at a constant 5 rpm or 8 rpm on the first trial (n = 8 in each). (C and D) Amount of time mice remained on the rotarod at a constant 10 rpm (n = 8 in each) (C) or 30 rpm (n = 7 in each) (D) over eight trials. (E) Ambulation count in the open field during 3 min (n = 6 to 7). Error bars represent the mean ± SEM.

thus indicating that the developmental elimination of surplus CF synapses on PCs was not impaired in the mutant mice.

Similar to FcγRIIB-deficient mice, the PPF ratio was significantly increased in CD3ε-deficient mice, while the PPD ratio was unchanged except at an interpulse interval of 20 ms (Fig. 3D and E). The developmental elimination of surplus CF synapses on PCs was not affected (Fig. 3F).

Poor rotarod performance in FcγRIIB-deficient and CD3ε-deficient mice. Finally, we assessed motor learning and motor coordination using the rotarod test in the two knockout mice. We first evaluated animals under standard conditions using an accelerating rotarod test (Fig. 4A). Rotarod speed increased from 2 rpm to 30 rpm within 5 min. On the first trial, the latencies at which the two mutant mice fell did not differ from those in the control mice. In all three strains, the latencies increased gradually as they gained experience (analysis of variance, $F_{7, 191} = 53.2$; $P < 0.0001$). As a whole, a strain effect did not reach a significant level ($F_{2, 191} = 2.3$; $P = 0.12$). However, the efficiency of improvements in the two mutant mice was lower in the latter four trials. During the first four trials, there was not a significant strain effect ($F_{2, 95} = 0.61$; $P = 0.55$). However, during the later four trials, a strain effect became evident ($F_{2, 95} = 7.0$; $P = 0.005$). Therefore, we hypothesized that the motor coordination evaluated in the first trial might not be changed, whereas the rising curve of the latency might be changed in the two mutant mice.

To confirm the hypothesis, we measured the latency in the first trial with constant rotarod speed. There were not significant differences at either 5 rpm or 8 rpm ($F_{2, 23} = 0.08$ [$P = 0.93$] and $F_{2, 23} = 0.12$ [$P = 0.89$], respectively) (Fig. 4B).

We next evaluated the rising curve of the latency at constant rotarod speed. When FcγRIIB-deficient and CD3ε-deficient mice were tested at a constant 10 rpm, they performed similarly to control mice ($F_{1, 103} = 0.02$ [$P = 0.90$] and $F_{1, 111} = 0.02$ [$P = 0.89$], respectively) (Fig. 4C). In contrast, the latencies were significantly shorter in the FcγRIIB-deficient and CD3ε-deficient mice at 30 rpm ($F_{1, 127} = 28.7$ [$P = 0.0001$] and $F_{1, 127} = 20.1$ [$P = 0.0005$], respectively) (Fig. 4D). General motor activities in the two mutant mice, as evaluated by ambulation count in the open field, were not significantly changed ($F_{2, 21} = 0.98$, $P = 0.39$) (Fig. 4E). Thus, the rotarod performance was impaired at high speed.

DISCUSSION

In the present investigation, both CD3ε-deficient and FcγRIIB-deficient mice showed an increased PPF ratio in PF-PC synapses. PPF is an event characteristic of synapses with low release probability of a neurotransmitter. As the PF terminals mature, the release probability is increased, resulting in a decrease in the PPF ratio. Thus, an increased PPF in CD3ε-deficient and FcγRIIB-deficient mice indicates a lowered release probability of PF terminals. In these mutant mice, rotarod performances were worse only at high speed. The motor learning ability of these two mutant mice did not seem to be affected, because there were no differences at a low rotarod speed. In the FcγRIIB-deficient mice, robust long-term depression was induced following conjunctive stimulation of PFs with PC depolarization in the cerebellum (data not shown), which might reflect the selective impairment in rotarod tasks. In the two mutant mice, the upper limit of learning capacity might be lowered. However, we cannot exclude the possibility that the mutant mice have difficulty in gripping the rotarod at high speed. Interestingly, similar impairments, poor rotarod performance and mild enhancement of the PPF ratio in PF-PC synapses, were also seen in mutant mice deprived of Munc13-3, a component of presynaptic active zones (2). Further studies are needed to determine whether poor rotarod performance is associated with modification of PF-PC synaptic functions in these mutant mice.

We found impaired architectures of PCs and GCs during development in the two mutant mice. The two molecules are expressed on the somata, dendrites, and spines of PCs. Lack of either of the two molecules on PCs might intrinsically contribute to the impaired development of PC dendrites. Presynaptic terminals of PFs make synaptic contacts with PC dendrites, and PFs exert instructive roles in the development of distal PC dendrites and in the planar organization of dendritic arbors. We found lesser VGLUT1 signals in the two mutant mice.

Therefore, the immature GC might also contribute to the impaired PC dendrites.

The two molecules were also found on the Bergmann glia. An increasing body of evidence suggests the participation of Bergmann glia in the development of cerebellar neurons as a scaffold for the migration and positioning of cerebellar neurons (31). It is also possible that the two molecules on the Bergmann glia influenced the development of cerebellar neurons. However, the size of cultured astrocytes from the two mutant mice was not essentially altered compared to the control mice (data not shown).

We describe a role of immune molecules in the cerebellum in vivo. In the immune system, the two molecules are expressed in different immune cells. CD3ε is exclusively expressed on T cells, where the TCR-CD3 complex recognizes specific antigens bound to MHC on APCs and forms immunological synapses. Among CD3 subunits, roles of CD3ζ in the brain have been studied in vivo. CD3ζ is expressed in neurons, such as the LGN and hippocampus (3, 8). In CD3ζ mutant mice, refinement of connections between the retina and central targets during development was incomplete. These results indicate a crucial role for CD3ζ in functional weakening and structural retraction of synaptic connections in the LGN and hippocampus (3, 8). On the other hand, we showed unexpected roles of CD3ε, -γ, and/or -δ in the cerebellum because we used CD3ε-deficient mice, in which CD3δ is also not detected, and the CD3γ protein level was reduced (16). Our results and those with CD3ζ mutant mice suggest that the ligand for CD3 subunits exists in the brain. It remains elusive whether a common molecule acts as a ligand for both CD3ζ and other CD3 subunits. Recently, paired immunoglobulin-like receptor B (PirB), an MHC class I receptor, was found to be expressed in subsets of neurons throughout the brain, and in mutant mice lacking functional PirB, cortical ocular dominance plasticity is more robust at all ages (27). Although antigen/MHC complex is the ligand of the TCR-CD3 complex in T cells, it seems to be unlikely that MHC antigen is a ligand for CD3ε, -γ, and/or -δ in the cerebellum, because mice lacking surface expression of MHC class I and MHC class II knockout mice performed normally in a rotarod test (data not shown), and the TCRα transcript was not detected in the brain (21, 28). Unlike in the LGN and hippocampus, CD3ζ is absent in the cerebellum. The current model of TCR-CD3 signaling in T cells assumes phosphorylation of the ITAMs in CD3ζ and subsequent involvement of several molecules, such as ZAP-70, SLP76, Vav, Nck, and WASP, for actin polymerization (13). Therefore, other molecules might associate with CD3ε, -γ, and/or -δ in the cerebellum. FcRγ was a candidate because it has an ITAM and is included in the CD3 complex in T cells in the intestine of CD3ζ knockout mice (14, 17). However, the performances of FcRγ knockout mice in the rotarod test were comparable with those of control mice (data not shown). Rather, ITAM-independent signaling would function in the cerebellum.

FcγRIIB shows a different pattern of expression than CD3 in the immune system. FcγRIIB is broadly distributed on hematopoietic cells (29) but not on mature T cells. In immune cells, it inhibits various cellular functions, such as B-cell activation, antigen presentation, cell proliferation, and antibody production (29). FcγRIIB might also reduce the development of autoimmune disease. The lack of FcγRIIB enhanced susceptibility to myelin oligodendrocyte glycoprotein-induced autoimmune experimental allergic encephalitis and increased the extent of demyelination (1). Thus, the functions of FcγRIIB are different from those of CD3 in the immune system. In contrast, we demonstrated a common physiological role of the two molecules in the development of the cerebellum. FcRγ, another immunoglobulin G Fc receptor subunit, is pivotal to the differentiation of oligodendrocyte precursor cells into myelinating oligodendrocytes (19). Therefore, the roles of immunoglobulin G Fc receptors in the development of the brain are diverse. Further studies will elucidate the neuron-specific signaling of FcγRIIB and CD3.

ACKNOWLEDGMENTS

FcγRIIB knockout mice were kindly provided by T. Takai (Tohoku University).

We declare that none of the authors has financial interests.

This work was supported in part by research grants from the Ministry of Education, Science, Technology, Sports and Culture of Japan.

REFERENCES

1. **Abdul-Majid, K. B., A. Stefferl, C. Bourquin, H. Lassmann, C. Linington, T. Olsson, S. Kleinau, and R. A. Harris.** 2002. Fc receptors are critical for autoimmune inflammatory damage to the central nervous system in experimental autoimmune encephalomyelitis. Scand. J. Immunol. **55**:70–81.
2. **Augustin, I., S. Korte, M. Rickmann, H. A. Kretzschmar, T. C. Sudhof, J. W. Herms, and N. Brose.** 2001. The cerebellum-specific Munc13 isoform Munc13-3 regulates cerebellar synaptic transmission and motor learning in mice. J. Neurosci. **21**:10–17.
3. **Corriveau, R. A., G. S. Huh, and C. J. Shatz.** 1998. Regulation of class I MHC gene expression in the developing and mature CNS by neural activity. Neuron **21**:505–520.
4. **Crepel, F., J. Mariani, and N. Delhaye-Bouchaud.** 1976. Evidence for a multiple innervation of Purkinje cells by climbing fibers in the immature rat cerebellum. J. Neurobiol. **7**:567–578.
5. **Dustin, M. L., and J. A. Cooper.** 2000. The immunological synapse and the actin cytoskeleton: molecular hardware for T cell signaling. Nat. Immunol. **1**:23–29.
6. **Hayes, S. M., and P. E. Love.** 2002. Distinct structure and signaling potential of the gamma delta TCR complex. Immunity **16**:827–838.
7. **Hirai, H., T. Launey, S. Mikawa, T. Torashima, D. Yanagihara, T. Kasaura, A. Miyamoto, and M. Yuzaki.** 2003. New role of δ2-glutamate receptors in AMPA receptor trafficking and cerebellar function. Nat. Neurosci. **6**:869–876.
8. **Huh, G. S., L. M. Boulanger, H. Du, P. A. Riquelme, T. M. Brotz, and C. J. Shatz.** 2000. Functional requirement for class I MHC in CNS development and plasticity. Science **290**:2155–2159.
9. **Ichihara, K., T. Nabeshima, and T. Kameyama.** 1993. Dopaminergic agonists impair latent learning in mice: possible modulation by noradrenergic function. J. Pharmacol. Exp. Ther. **264**:122–128.
10. **Jacobs, H.** 1997. Pre-TCR/CD3 and TCR/CD3 complexes: decamers with differential signalling properties? Immunol. Today **18**:565–569.
11. **Jiao, Y., J. Yan, Y. Zhao, L. R. Donahue, W. G. Beamer, X. Li, B. A. Roe, M. S. Ledoux, and W. Gu.** 2005. Carbonic anhydrase-related protein VIII deficiency is associated with a distinctive lifelong gait disorder in waddles mice. Genetics **171**:1239–1246.
12. **Kato, K.** 1990. Sequence of a novel carbonic anhydrase-related polypeptide and its exclusive presence in Purkinje cells. FEBS Lett. **271**:137–140.
13. **Lin, J., and A. Weiss.** 2001. T cell receptor signalling. J. Cell Sci. **114**:243–244.
14. **Liu, C. P., R. Ueda, J. She, J. Sancho, B. Wang, G. Weddell, J. Loring, C. Kurahara, E. C. Dudley, A. Hayday, et al.** 1993. Abnormal T cell development in CD3-$\zeta^{-/-}$ mutant mice and identification of a novel T cell population in the intestine. EMBO J **12**:4863–4875.
15. **Loconto, J., F. Papes, E. Chang, L. Stowers, E. P. Jones, T. Takada, A. Kumanovics, K. Fischer Lindahl, and C. Dulac.** 2003. Functional expression of murine V2R pheromone receptors involves selective association with the M10 and M1 families of MHC class Ib molecules. Cell **112**:607–618.
16. **Malissen, M., A. Gillet, L. Ardouin, G. Bouvier, J. Trucy, P. Ferrier, E. Vivier, and B. Malissen.** 1995. Altered T cell development in mice with a targeted mutation of the CD3-epsilon gene. EMBO J. **14**:4641–4653.
17. **Malissen, M., A. Gillet, B. Rocha, J. Trucy, E. Vivier, C. Boyer, F. Kontgen, N. Brun, G. Mazza, E. Spanopoulou, et al.** 1993. T cell development in mice lacking the CD3-zeta/eta gene. EMBO J **12**:4347–4355.
18. **Miyazaki, T., M. Fukaya, H. Shimizu, and M. Watanabe.** 2003. Subtype

switching of vesicular glutamate transporters at parallel fibre-Purkinje cell synapses in developing mouse cerebellum. Eur. J. Neurosci. **17**:2563–2572.
19. **Nakahara, J., K. Tan-Takeuchi, C. Seiwa, M. Gotoh, T. Kaifu, A. Ujike, M. Inui, T. Yagi, M. Ogawa, S. Aiso, T. Takai, and H. Asou.** 2003. Signaling via immunoglobulin Fc receptors induces oligodendrocyte precursor cell differentiation. Dev. Cell **4**:841–852.
20. **Nakamura, M., K. Sato, M. Fukaya, K. Araishi, A. Aiba, M. Kano, and M. Watanabe.** 2004. Signaling complex formation of phospholipase Cβ4 with metabotropic glutamate receptor type 1α and 1,4,5-trisphosphate receptor at the perisynapse and endoplasmic reticulum in the mouse brain. Eur. J. Neurosci. **20**:2929–2944.
21. **Nishiyori, A., Y. Hanno, M. Saito, and Y. Yoshihara.** 2004. Aberrant transcription of unrearranged T-cell receptor beta gene in mouse brain. J Comp. Neurol. **469**:214–226.
22. **Ono, M., H. Okada, S. Bolland, S. Yanagi, T. Kurosaki, and J. V. Ravetch.** 1997. Deletion of SHIP or SHP-1 reveals two distinct pathways for inhibitory signaling. Cell **90**:293–301.
23. **Pasterkamp, R. J., J. J. Peschon, M. K. Spriggs, and A. L. Kolodkin.** 2003. Semaphorin 7A promotes axon outgrowth through integrins and MAPKs. Nature **424**:398–405.
24. **Ravetch, J. V., A. D. Luster, R. Weinshank, J. Kochan, A. Pavlovec, D. A. Portnoy, J. Hulmes, Y. C. Pan, and J. C. Unkeless.** 1986. Structural heterogeneity and functional domains of murine immunoglobulin G Fc receptors. Science **234**:718–725.
25. **Reth, M.** 1989. Antigen receptor tail clue. Nature **338**:383–384.
26. **Shibata, T., K. Yamada, M. Watanabe, K. Ikenaka, K. Wada, K. Tanaka, and Y. Inoue.** 1997. Glutamate transporter GLAST is expressed in the radial glia-astrocyte lineage of developing mouse spinal cord. J. Neurosci. **17**:9212–9219.
27. **Syken, J., T. Grandpre, P. O. Kanold, and C. J. Shatz.** 2006. PirB restricts ocular-dominance plasticity in visual cortex. Science **313**:1795–1800.
28. **Syken, J., and C. J. Shatz.** 2003. Expression of T cell receptor beta locus in central nervous system neurons. Proc. Natl. Acad. Sci. USA **100**:13048–13053.
29. **Takai, T.** 2002. Roles of Fc receptors in autoimmunity. Nat. Rev. Immunol. **2**:580–592.
30. **Takai, T., M. Ono, M. Hikida, H. Ohmori, and J. V. Ravetch.** 1996. Augmented humoral and anaphylactic responses in Fc gamma RII-deficient mice. Nature **379**:346–349.
31. **Yamada, K., M. Fukaya, T. Shibata, H. Kurihara, K. Tanaka, Y. Inoue, and M. Watanabe.** 2000. Dynamic transformation of Bergmann glial fibers proceeds in correlation with dendritic outgrowth and synapse formation of cerebellar Purkinje cells. J. Comp. Neurol. **418**:106–120.

Available online at www.sciencedirect.com
ScienceDirect
Prostaglandins, Leukotrienes and Essential Fatty Acids 76 (2007) 321–329
Prostaglandins Leukotrienes Essential Fatty Acids
www.elsevier.com/locate/plefa

Simultaneous quantification of seven prostanoids using liquid chromatography/tandem mass spectrometry: The effects of arachidonic acid on prostanoid production in mouse bone marrow-derived mast cells ☆

Takanori Hishinuma[a], Kaori Suzuki[a], Masayoshi Saito[a], Hiroaki Yamaguchi[a], Naoto Suzuki[b], Yoshihisa Tomioka[b], Izumi Kaneko[c], Masao Ono[c], Junichi Goto[a,d,*]

[a]*Graduate School of Pharmaceutical Sciences, Tohoku University*
[b]*Faculty of Pharmaceutical Sciences, Josai International University*
[c]*Department of Pathology, Tohoku University Graduate School of Medicine*
[d]*Department of Pharmaceutical Sciences, Tohoku University Hospital*

Received 13 December 2006; received in revised form 23 March 2007; accepted 4 April 2007

Abstract

We have developed a method for the simultaneous estimation of the levels of the prostanoids 6-keto prostaglandin (PG) $F_{1\alpha}$, PGB_2, PGD_2, PGE_2, $PGF_{2\alpha}$, PGJ_2, and thromboxane (TX) B_2 in blood- or serum-containing medium using liquid chromatography-tandem mass spectrometry. These prostanoids and their deuterium derivatives, which were used as internal standards, were subjected to solid-phase extraction using Empore C18 HD disk cartridges and analyzed in the selected reaction-monitoring mode. A linear response curve starting at 10 pg of prostanoid/tube was observed for each prostanoid. The accuracy of the method was demonstrated with samples containing known amounts of the prostanoids. Furthermore, we used this method to analyze the prostanoids produced in mouse bone marrow-derived mast cells stimulated with arachidonic acid, which resulted in the production of PGD_2, PGE_2, $PGF_{2\alpha}$, and TXB_2. The results suggest that this simultaneous quantification method is useful for the analysis of the production of biomedically important prostanoids.

1. Introduction

Prostanoids are bioactive lipid mediators that are synthesized from arachidonic acid (AA) via the arachidonate cascade. These molecules, which play vital roles in a variety of physiological and pathophysiological conditions, are produced in various tissues and cells *in vivo*. Despite their similar molecular structures, prostanoids have different biological effects [1–7]. For example, prostaglandin (PG) E_2 contributes to inflammation and carcinogenesis [6]. On the other hand, PGD_2 induces bronchocontriction, acts as an allergic mediator [7], and functions as a neurotransmodulator of several centrally controlled functions, such as the sleep–wake cycle [8]. Cyclopentenone prostaglandins are dehydration products of either PGD_2 or PGE_2; dehydration of PGD_2 results in the formation of PGJ_2, whereas dehydration of PGE_2 produces PGB_2. There has been significant recent interest in the roles that cyclopente-

☆A part of this research was supported by Grant-in-Aid for Strategic Japanese-Swedish Cooperative Program on "Multidisciplinary Bio" from Japan Science and Technology Agency, Grant-in-Aid for Scientific Research(B) and Exploratory Research from Ministry of Education, Japan.
*Corresponding author. Department of Pharmaceutical Sciences, Tohoku University Hospital, 1-1 Seiryo-machi, Aoba-ku, Sendai 980-8574, Japan. Tel.: +81 22 717 7527; fax: +81 22 717 7545.
E-mail address: junlgoto@mail.tains.tohoku.ac.jp (J. Goto).

0952-3278/$ - see front matter © 2007 Elsevier Ltd. All rights reserved.
doi:10.1016/j.plefa.2007.04.005

none prostaglandins play in cellular proliferation and differentiation [9,10]. Thromboxane (TX) A_2, and PGI_2, which have short half-lives, are automatically converted to TXB_2 [11,15] and 6-keto $PGF_{1\alpha}$ [11], respectively. TXA_2 has aggregatory and vasoconstrictor effects [6,15]. In contrast, PGI_2 has antiaggregatory and vasodilator effects [11]. $PGF_{2\alpha}$ contributes to parturition and bronchocontriction [1,6,7]. In addition, these prostanoids have pathological effects; the abnormalities they produce have been implicated in a wide range of diseases, including diabetic vascular complications [11–15], atherosclerosis [15], allergic asthma [7,16], rheumatoid arthritis [17], and renal diseases [18]. Despite these observations, the mechanisms that contribute to the production of prostanoids have yet to be clarified. Therefore, a reliable microdetermination method would be very useful for investigations of the functions of PGs in these diseases.

The quantification of prostanoids is generally performed using high-performance liquid chromatography (HPLC) together with a radioimmunoassay or enzyme linked immunosorbent assay. These techniques, however, are associated with a variety of problems, including the use of a radioactive compound, complicated procedures, low sensitivities, poor specificities, cross-reactivity, and complicated clean-up procedures to eliminate interfering substances from biological samples. Additionally, these methods are limited to the detection of a single product at a time. Gas chromatography/selected ion monitoring (GC/SIM) is more sensitive and specific than an immunoassay. Moreover, these methods can be used for the simultaneous quantification of prostanoids [19,20]. The GC/SIM technique, however, requires a complicated derivation procedure.

Mass spectrometry (MS) coupled with liquid chromatography (LC) is sufficiently dependable for reliable sample analysis. In particular, liquid chromatography/tandem mass spectrometry (LC/MS/MS) performed using an electrospray ionization (ESI) interface is a powerful technique that allows for highly specific and quantitative measurement of various compounds in a variety of biological samples [21]. Recently, methods for the quantification of AA metabolites using LC/MS/MS have been reported [22–38]. Some of these methods, however, are not suitable for clinical serum samples and medium containing fetal bovine serum (FBS); many of them require that the serum-containing medium be replaced with serum-free medium. In culture-free medium, however, cells may not perform their native functions.

Membrane lipid metabolites, such as prostaglandins, have been characterized as early mediators that influence the activation of bone marrow-derived mast cells (mBMMCs) [39–41] and the onset of allergic inflammation in murine models [42,43]. The application of LC/MS/MS to PG production in mBMMCs may be useful for the pathologic analysis of allergies and inflammatory affections.

In this study, we established a simple and effective simultaneous quantification method for seven prostanoids using simple solid-phase extraction and LC/MS/MS performed in the selected reaction-monitoring (SRM) mode. Moreover, we detailed the extraction steps required to obtain a level of sensitivity that allows the detection of prostanoid production in serum-containing medium. We then measured the effects of AA on prostanoid production in mBMMCs in the presence of FBS.

2. Materials and methods

2.1. Materials

6-Keto $PGF_{1\alpha}$, 6-keto $PGF_{1\alpha}$-d_4, PGB_2, PGB_2-d_4, PGD_2, PGD_2-d_4, PGE_2, PGE_2-d_4, $PGF_{2\alpha}$, $PGF_{2\alpha}$-d_4, PGJ_2, TXB_2, and TXB_2-d_4 were purchased from Cayman Co. (USA). Other solvents and reagents were of the highest quality available. Empore C18 HD disk cartridges (7 mm/3 mL) were purchased from the Industrial and Consumer sector of 3 M (USA). HPLC-grade solvents were obtained from Wako Pure Chemical Industries (Osaka, Japan).

2.2. LC/MS/MS analysis

The LC/MS/MS system was a Quattro II triple–quadrupole tandem mass spectrometer (Micromass, Manchester, UK) equipped with an ESI interface operated in the negative-ion mode. A nanospace SI-1 HPLC system (Shiseido, Tokyo, Japan) was used. Chromatography was performed on a C18 Capcell Pak UG120 column (Shiseido, Tokyo, Japan; 1.5 × 150 mm, 3 μm) using isocratic elution with acetonitrile–water–acetic acid (40:60:0.02, v/v/v) at a flow rate of 100 μL/min. The column was maintained at 40 °C. Column effluent was introduced into the mass spectrometer between 2 and 14 min after injection using a fused silica capillary.

SRM was performed by monitoring the transitions summarized in Table 1. The thickness of the collision gas (argon) was 1.0×10^{-3} mbar. The capillary voltage was −3500 V. Cone voltage and collision energy were optimized for each compound to obtain optimum sensitivity. The source temperature was 160 °C. Peak areas and calibration curves were obtained using the MassLynx program (Micromass, Manchester, UK).

2.3. Cell culture and extraction procedure

mBMMCs were prepared from suspension cell cultures of bone marrow obtained from young C57BL/

6J male mice (Charles River Japan, Yokohama, Japan). mBMMCs were cultured in RPMI1640 medium containing 10% FBS, 100 U/mL penicillin G, 100 μg/mL streptomycin, 1 mM sodium pyruvate, 1x nonessential amino acids (Sigma, St. Louis, MO), 5 ng/mL murine IL-3 (R&D Systems, Minneapolis, MN), and 50 μM 2-mercaptoethanol at 37 °C under a 95%/5% air/CO_2 atmosphere. For the experiments, we used mBMMC populations in which more than 95% of the cells were positive for IgE binding and c-KIT as measured using flow cytometry.

Table 1
Selected reaction monitoring (SRM) transitions for the liquid chromatography/tandem mass spectrometry (LC/MS/MS) determination of prostanoids

Compound	SRM (m/z)	Cone voltage (V)	Collission energy (eV)
6-keto $PGF_{1\alpha}$	369→163	−30	25
6-keto $PGF_{1\alpha}$-d_4	373→167	−30	25
PGB_2	333→175	−50	20
PGB_2-d_4	337→179	−50	20
PGD_2	351→189	−35	20
PGD_2-d_4	355→193	−35	20
PGE_2	351→271	−35	15
PGE_2-d_4	355→275	−35	15
$PGF_{2\alpha}$	353→193	−50	25
$PGF_{2\alpha}$-d_4	357→197	−50	25
PGJ_2	333→189	−30	20
TXB_2	369→195	−40	15
TXB_2-d_4	373→195	−40	15

mBMMCs (1×10^5 cells/200 μL) were cultured with AA (25 μg/mL). After 24 h of incubation, 200 μL of cultured medium was harvested and assayed. To each 200-μL sample of cultured medium, 6-keto $PGF_{1\alpha}$-d_4, PGB_2-d_4, PGD_2-d_4, PGE_2-d_4, $PGF_{2\alpha}$-d_4, and TXB_2-d_4 (1 ng each) were added as internal standards. The sample was adjusted to pH 4.0 with 1 M HCl and was passed through an Empore C18 HD disk cartridge, which was preconditioned with methanol (2 mL) followed by distilled water (2 mL). The cartridge was washed with distilled water (4 mL) and hexane (4 mL), to remove peptides and salts as well as polar and nonpolar interfering substances. 6-Keto $PGF_{1\alpha}$, PGB_2, PGD_2, PGE_2, $PGF_{2\alpha}$, PGJ_2, and TXB_2 were eluted with hexane/ethyl acetate (1:2, v/v, 1 mL) in a siliconized glass tube to avoid absorption by the tube. After evaporating the solvent, the residue was reconstituted in the mobile phase (40 μL), sonicated for 30 s, and filtrated. The sample was then transferred

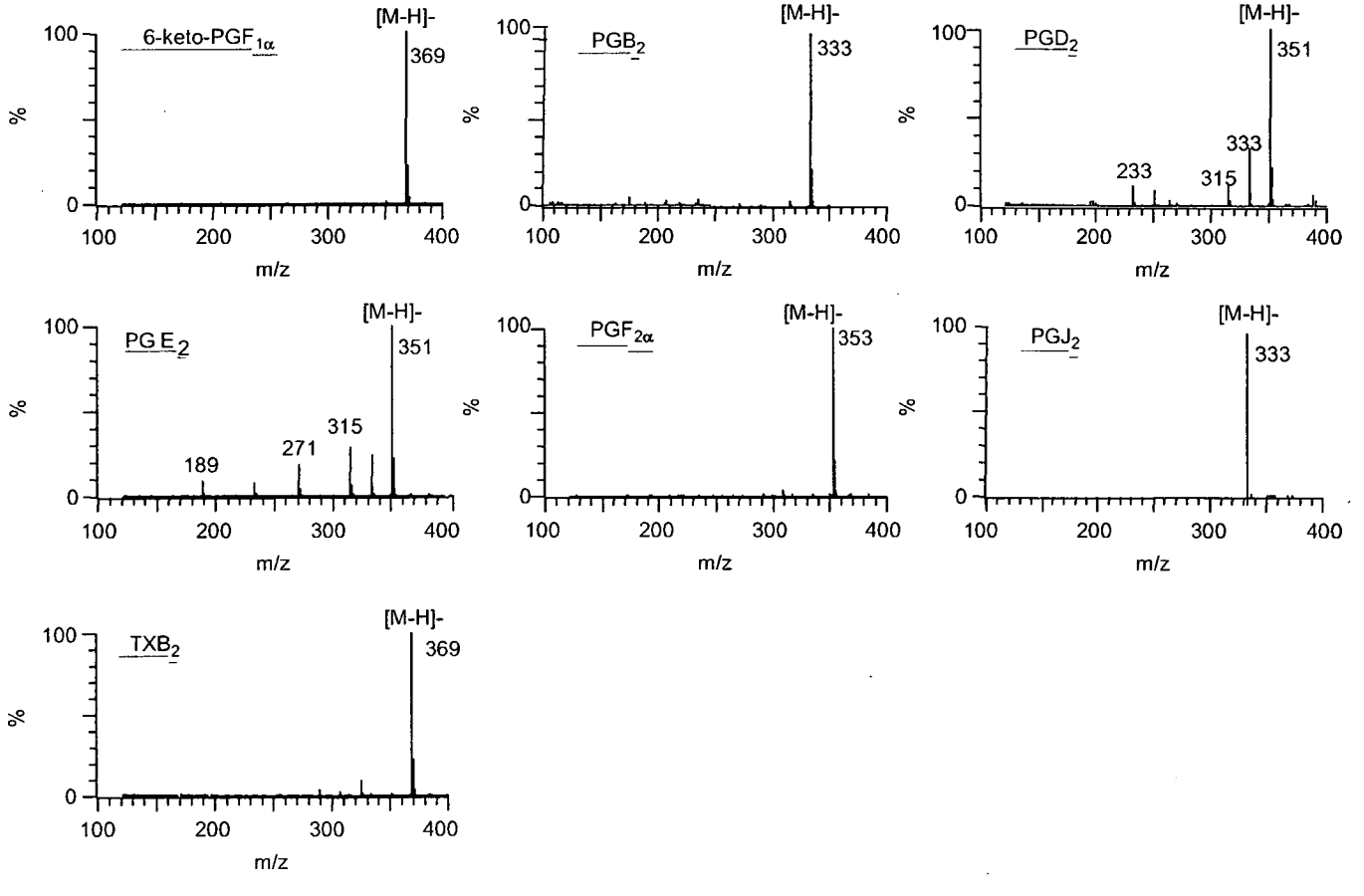

Fig. 1. Mass spectra of the prostanoids.

to an autosampler vial, and 10 μL was injected for LC/MS/MS.

3. Results

3.1. Mass and product ion mass spectra

The mass spectra of 6-keto $PGF_{1\alpha}$, 6-keto $PGF_{1\alpha}$-d_4, PGB_2, PGB_2-d_4, PGD_2, PGD_2-d_4, PGE_2, PGE_2-d_4, $PGF_{2\alpha}$, $PGF_{2\alpha}$-d_4, PGJ_2, TXB_2, and TXB_2-d_4 were obtained (Fig. 1). Each base peak corresponded to the respective deprotonated molecule ($[M-H]^-$). Because prostanoids contain free carboxylic acid groups, ESI results in abundant carboxylate ions. The product ion mass spectra of both the analyte and its internal standard were obtained by choosing the deprotonated molecules as the precursor ions (Fig. 2). Table 1 shows the optimal cone voltage, collision energy, and ion pairs selected for LC/MS/MS determination of each of the compounds.

3.2. Selected reaction-monitoring

In addition to affecting separation on LC, changes in the mobile phase composition can alter the sensitivity of MS by influencing the ionization efficiency of 6-keto $PGF_{1\alpha}$, PGB_2, PGD_2, PGE_2, $PGF_{2\alpha}$, PGJ_2, or TXB_2. Therefore, we first needed to optimize the mobile phase to obtain a high degree of sensitivity, good separation, and a short analysis time. A high degree of sensitivity on MS was concurrently observed with good separation on LC when an acetonitrile/water/acetic acid (40:60:0.02, v/v/v) mobile phase was used. Moreover, this composition also resulted in a short analysis time (Fig. 3).

After optimization of the mobile phase, we tried to detect 6-keto $PGF_{1\alpha}$, PGB_2, PGD_2, PGE_2, $PGF_{2\alpha}$, PGJ_2, and TXB_2 using LC/MS in the selected-ion monitoring (SIM) mode. In the SIM mode, however, attempts to monitor the respective deprotonated molecules for 6-keto $PGF_{1\alpha}$, PGB_2, PGD_2, PGE_2, $PGF_{2\alpha}$, PGJ_2, and TXB_2 failed to produce peaks due to the high background noise level. Therefore, we used LC/MS/MS in the SRM mode. With this method, the background noise level was remarkably reduced and sharp peaks corresponding to 6-keto $PGF_{1\alpha}$, PGB_2, PGD_2, PGE_2, $PGF_{2\alpha}$, PGJ_2, and TXB_2 were observed. Moreover, because we used a semi-micro HPLC system, which included a switching-valve unit to introduce the column effluent for a very brief period of time, only a small sample was required. This meant that the mass spectrometer remained relatively clean and, consequently, the background noise level on the chromatograms was low.

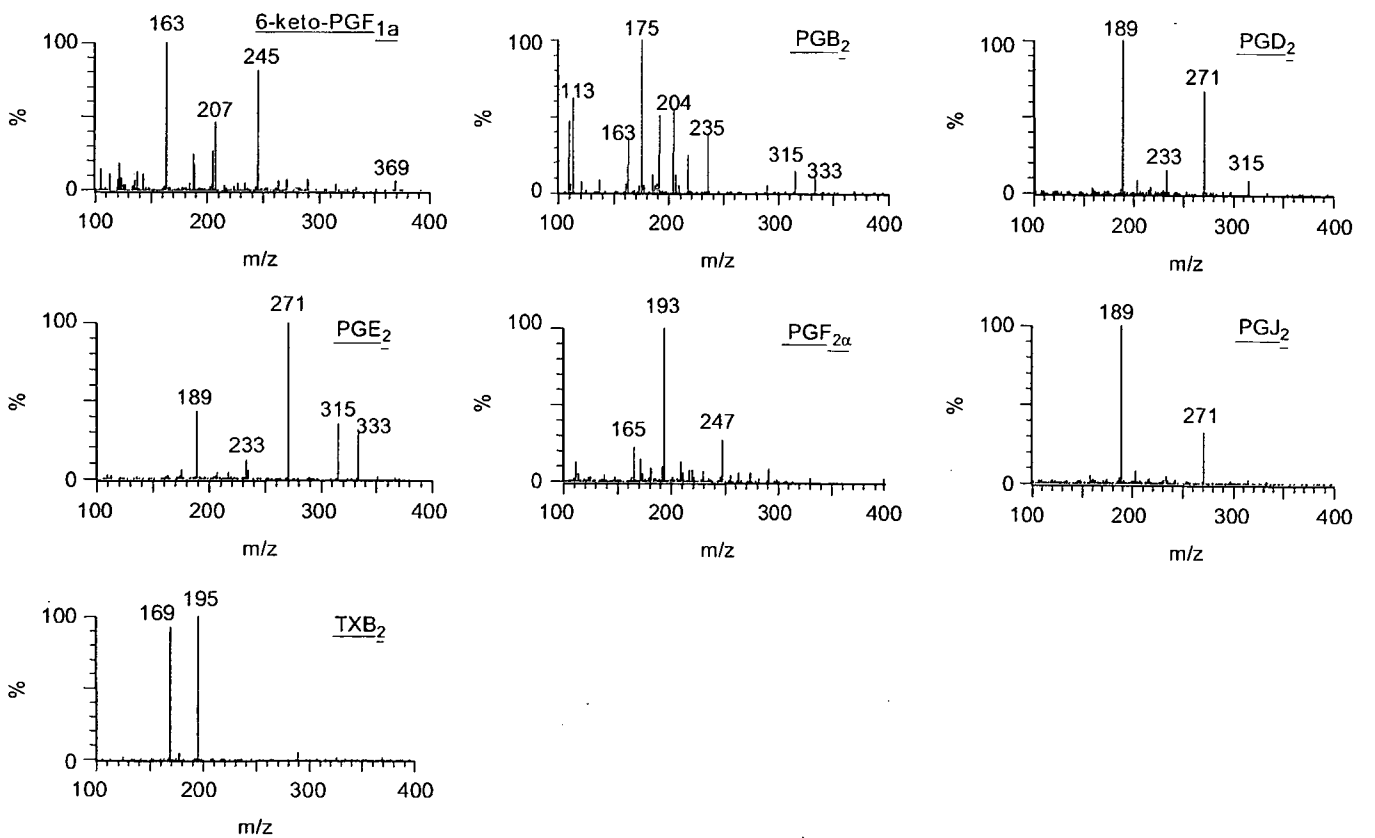

Fig. 2. Product ion mass spectra of the prostanoids.

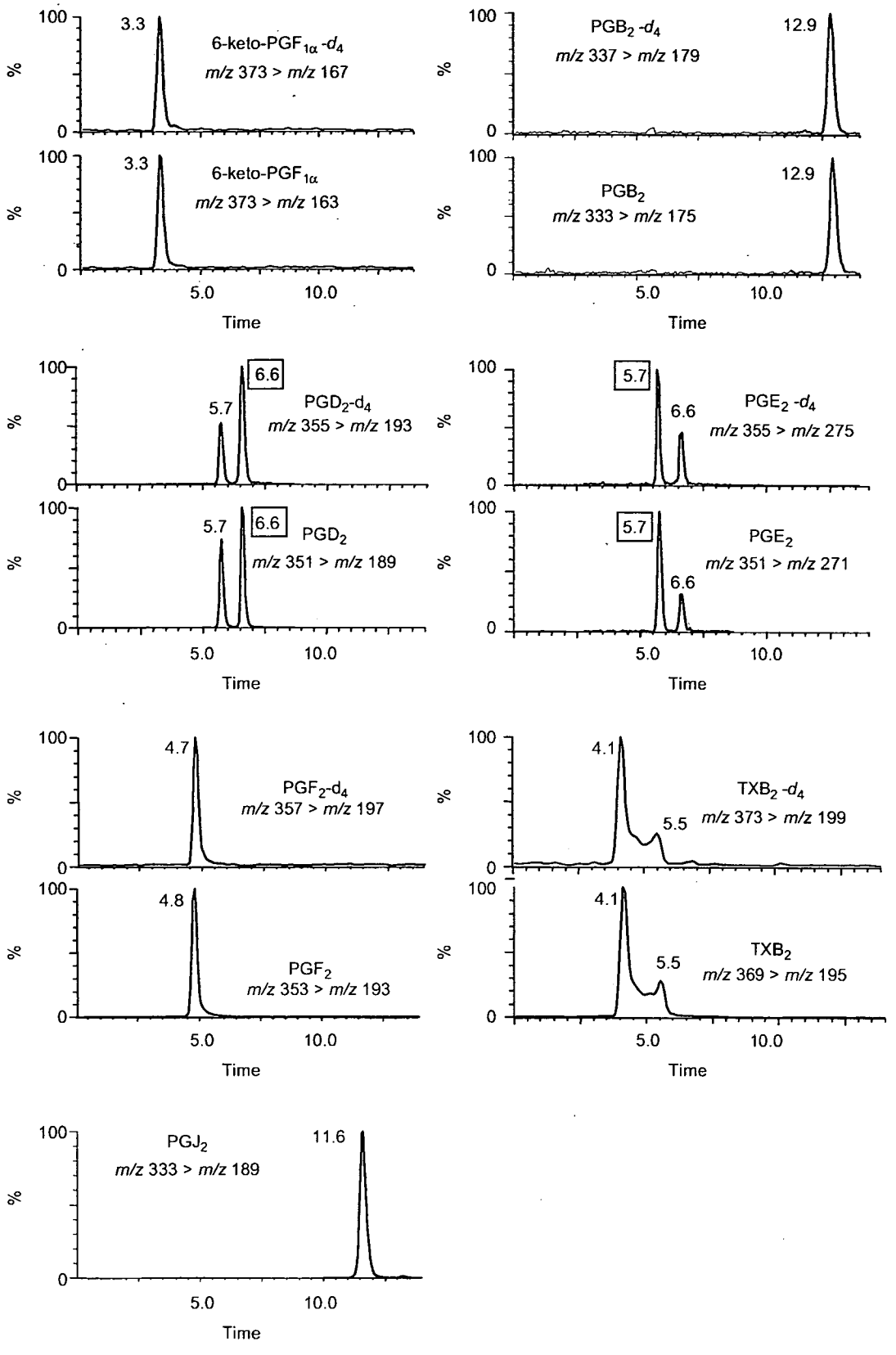

Fig. 3. SRM chromatograms of the prostanoids.

3.3. Calibration curve

A calibration curve for PGE_2 was generated in the SRM using increasing known amounts of PGE_2 and a constant level of PGE_2-d_4 as the internal standard (1). Calibration standards were prepared in triplicate. A linear calibration curve was constructed using least-squares regression quantities vs. the ratio of the peak area to that of the peak corresponding to PGE_2-d_4. 6-keto $PGF_{1\alpha}$, PGB_2, PGD_2, $PGF_{2\alpha}$, and TXB_2 were analyzed using the same method. PGB_2-d_4 was used as an internal standard for the quantitation of both PGB_2 and PGJ_2, because these molecules display similar chromatographic behaviors. The curves for these PGs were relatively linear in the range from 10 pg/tube to 10 ng/tube ($r = 0.999$).

3.4. Accuracy

After the addition of an internal standard to the cell culture medium, three samples were subjected to the sample preparation procedure to demonstrate the experimental reproducibility (Table 2). Statistical analysis was carried out using one-way analysis of variance [44] to separate the analytical errors arising from two sources: sample preparation and LC/MS/MS in the SRM mode. As shown in Table 3A, there was no significant contribution to the total variance from the sample preparation, whereas the coefficient of variation for LC/MS/MS in the SRM mode was 0.66%.

To examine the accuracy and the precision of the present method, cell culture medium spiked with 100, 200, 300, 500, or 1000 pg/tube was prepared. These samples were analyzed in triplicate. The results for PGE_2 are shown in Table 2. The accuracy of the measurements of the added prostanoids ranged between 98.7% and 104%. The coefficients of variation of the analyses of the prostanoids at 100, 200, 300, 500, or 1000 pg/tube ranged from 0.14% to 3.3%, whereas the absolute recovery level of the prostanoids ranged from 80.3% to 95.7%. Statistical analysis was carried out using two-way analysis of variance [44] to separate the analytical errors between sources: sample preparation and LC/MS/MS in the SRM mode. The findings indicate that there was no significant contribution to the total variance from spiking errors or sample preparation (Table 3B). Almost all of the variance in these experiments was attributed to LC/MS/MS in the SRM mode, because the errors from sample preparation and the concentrations of the prostanoids were negligible. These findings suggested that this simultaneous quantification method is highly reliable with good accuracy and precision.

Table 2
Accuracy of PGE_2 spiked cell culture media

	Mean level (pg/2 mL, $n = 3$)	Accuracy (%)	C.V. (%)
Non-spiked	Not detected		
+100 pg	100 ± 1.7	101 ± 1.7	1.69
+200 pg	201 ± 0.94	100 ± 0.47	0.470
+300 pg	300 ± 1.7	99.9 ± 0.57	0.567
+500 pg	501 ± 2.5	100 ± 0.50	0.498
+1000 pg	1001 ± 2.1	100 ± 0.21	0.205

Table 3
Analysis of variance

Source	S	f	V	F_0
(A) *Analysis of variance from the reproducibility test*				
Sample preparation	20.0	3	6.68	2.20
LC/MS/MS	24.3	8	3.03	–
Total	44.3	11	–	–
$F(3,8,0.05) = 4.07$				
(B) *Analysis of variance from the accuracy test*				
Spiking error (a)	3.98	4	0.955	0.955
Sample preparation (b)	3.87	2	1.94	1.94
a × b	23.2	8	2.90	2.90
LC/MS/MS	30.0	30	1.00	–
Total	61.0	44	–	–
$F(4,30,0.05) = 2.690$				
$F(2,30,0.05) = 3.316$				

S = residual sum of squares; F = number of degrees of freedom; $f_1 = f$ sample preparation; $f_2 = f$ error; V = unbiased variance; F_0 = observed value following F distribution variance ratio (v sample preparation/V error); $F(f_2,F_1,\alpha)$ = density function of F distribution with f_1 and f_2 degrees of freedom.

3.5. Application to cell culture medium

We investigated the production of prostanoids in the mBMMCs in the presence of 25 μg/mL AA (Fig. 4). The mBMMCs without added AA produced $PGF_{2\alpha}$ and TXB_2. The levels of these prostanoids, however, significantly increased following the addition of AA ($p < 0.05$). After the mBMMCs were incubated for 24 h in the presence of AA, the levels of the detected prostanoids were as follows: $TXB_2 > PGD_2 > PGE_2 \approx PGF_{2\alpha}$. 6-Keto $PGF_{1\alpha}$, PGB_2, and PGJ_2 were not detected.

4. Discussion

MS is a powerful technique that can provide highly specific and quantitative measurements of low levels of endogenous biological substances. Recently, LC coupled with MS has been successfully used for pharmaceutical analyses and quantification, because LC/MS combines the separation of the analytes on a LC column and the detection of ions using a mass

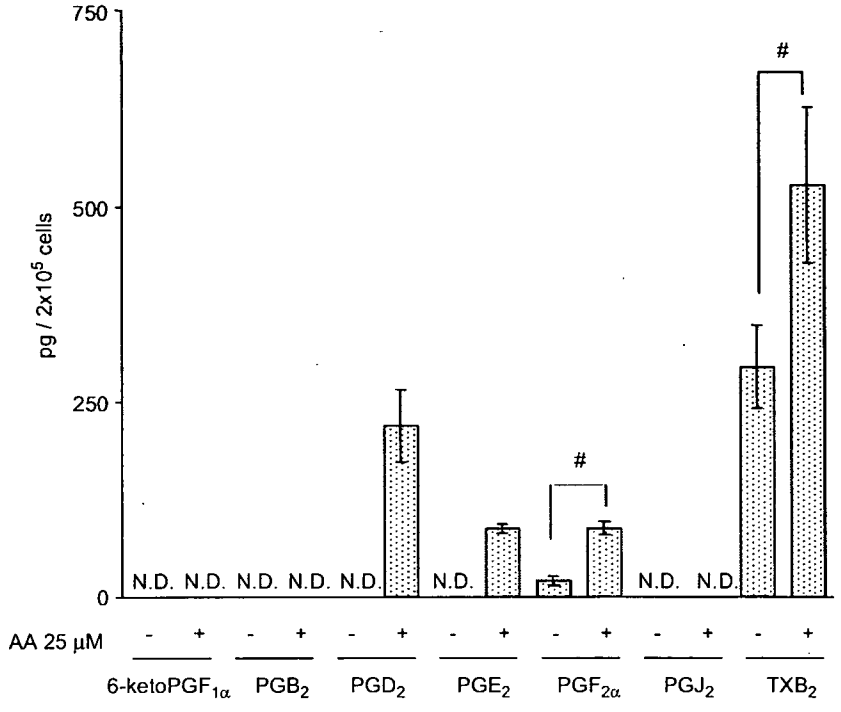

Fig. 4. Effect of AA on prostanoid production in mBMMCs. The mBMMCs (1×10^6 cells/mL) were cultured with AA (25 μg/mL). After 24 h of incubation, 200 μL of medium was harvested and assayed. 6-Keto $PGF_{1\alpha}$-d_4, PGB_2-d_4, PGD_2-d_4, PGE_2-d_4, $PGF_{2\alpha}$-d_4, and TXB_2-d_4 (1 ng each) were added to each 200-μL sample of cultured medium as internal standards. Prostanoids were extracted using Empore C18 HD disk cartridges and analyzed using LC/MS/MS as described in the Materials and Methods section.

spectrometer. For the determination of a wide variety of nonvolatile or thermally labile molecules, such as prostanoids, LC/MS and LC/MS/MS are especially useful. In addition, because of its sensitivity and specificity, LC/MS/MS is well suited for the analysis of prostanoids. With the SRM mode, it is possible to choose and monitor specific fragment ions for each prostanoid to identify and quantify the substrate more sensitively and specifically.

Microdetermination methods for eicosanoids using LC/MS/MS have been reported previously [23–38]. In the present study, we have developed a method for the simultaneous analysis of 6-keto $PGF_{1\alpha}$, PGB_2, PGD_2, PGE_2, $PGF_{2\alpha}$, PGJ_2, and TXB_2 using LC/MS/MS after a simple solid-phase extraction step to clean up the samples. An Empore C18 disk cartridge was used for the extraction of 6-keto $PGF_{1\alpha}$, PGB_2, PGD_2, PGE_2, $PGF_{2\alpha}$, PGJ_2 and TXB_2 from 200 μL of serum-containing medium. Before loading, the sample was acidified to increase the recovery rate by increasing the adsorptive activity. After the sample was loaded, the cartridge was washed with H_2O and hexane. This procedure, together with the use of minimal volumes of washing solvents, produced excellent clean-up results. This cartridge, which yielded good recovery even when a high flow rate was used during the sample loading and washing periods, required as little as 1 mL of elution solvent. Therefore, the time-consuming solvent evaporation step may be unnecessary. This feature is even more important for thermally labile compounds. Moreover, these methods can be used to clean up not only cell culture media, but also biological fluids. We have analyzed prostanoids in human sera and aqueous humor using these methods (data not shown). When tetradeuterium analogues were used as internal standards for each analyte, the present simultaneous quantification method was found to be highly accurate and precise. In the SRM chromatogram, the analyte peaks were well separated, indicating different retention times on the LC column, and no serious interfering peaks were detected. The analyte peaks were detected with retention times that were similar to those of their corresponding internal standards. Additionally, this good separation only required a simple LC system that employed an isocratic elution step. Therefore, our simultaneous quantification method, which has a fixed ionization efficiency, is more simple and reliable and than other previously published methods.

Calibration curves ranging from 10 pg/tube to 10 ng/tube exhibited good linearity. This range covered the levels of prostanoids produced by mBMMCs (2×10^5 cells). We found that mBMMCs without added AA produced $PGF_{2\alpha}$ and TXB_2. After a 24-h incubation in the presence of AA, however, the mBMMCs produced a variety of prostanoids ($TXB_2 > PGD_2 > PGE_2 \approx PGF_{2\alpha}$). In contrast, 6-keto $PGF_{1\alpha}$, PGB_2, and PGJ_2 were not

detected. Across the board, the levels we observed in these experiments were lower than those reported in other studies. This observation may be associated with the ages of the mBMMCs from the various studies. Activated mast cells produce a variety of chemical mediators. Among them, PGD_2 has been reported to be the major cyclooxygenase metabolite of AA, which is produced in response to a diverse range of stimuli [45,46]. A previous study reported that activated rat mast cells generate 6-keto $PGF_{1\alpha}$, PGD_2, PGE_2, $PGF_{2\alpha}$, and TXB_2 [47]. The finding that nonstimulated mBMMCs produce $PGF_{2\alpha}$, but not PGD_2 and PGE_2, however, is novel. The physiological roles of the production of prostanoids by mBMMCs should be elucidated in future studies. Our results suggest that this method will be useful for the investigation of prostanoid production by mBMMCs.

In conclusion, we have developed a rapid, highly specific, and highly sensitive LC/MS/MS-based method for the analysis of prostanoids in cell culture medium. This simultaneous quantification method is effective for the analysis of seven biologically important prostanoids and may be helpful for investigations of the mechanisms of prostanoid production. Because prostanoids have been implicated in numerous pathophysiological conditions, this method may also be of use in a variety of clinical settings.

References

[1] R.J. Helliwell, L.F. Adams, M.D. Mitchell, Prostaglandin synthases: recent developments and a novel hypothesis, Prostaglandins Leukot Essent. Fatty Acids 70 (2004) 101–113.

[2] R.J. Soberman, P. Christmas, The organization and consequences of eicosanoid signalling, J. Clin. Invest. 111 (2003) 1107–1113.

[3] C.D. Funk, Prostaglandins and leukotrienes: advances in eicosanoid biology, Science 294 (2001) 1871–1875.

[4] W.L. Smith, The eicosanoids and their biochemical mechanisms of action, Biochem. J. 259 (1989) 315–324.

[5] P. Needleman, J. Turk, B.A. Jakschik, A.R. Morrison, J.B. Lefkowith, Arachidonic acid metabolism, Annu. Rev. Biochem. 55 (1986) 69–102.

[6] W.L. Smith, R. Langenbach, Why there are two cyclooxygenase isozymes, J. Clin. Invest. 107 (2001) 1491–1495.

[7] L. Pang, A. Pitt, D. Petkova, A.J. Knox, The COX-1/COX-2 balance in asthma, Clin. Exp. Allergy 28 (1998) 1050–1058.

[8] Y. Urade, T. Tanaka, N. Eguchi, M. Kikuchi, H. Kimura, H. Toh, O. Hayaishi, Structural and functional significance of cysteine residues of glutathione-independent prostaglandin D synthase. Identification of Cys65 as an essential thiol, J. Biol. Chem. 270 (1995) 1422–1428.

[9] M. Fukushima, Biological activities and mechanisms of action of PGJ2 and related compounds: an update, Prostaglandins Leukot Essent. Fatty Acids 47 (1992) 1–12.

[10] R. Chinery, R.J. Coffey, R. Graves-Deal, S.C. Kirkland, S.C. Sanchez, W.E. Zackert, J.A. Oates, J.D. Morrow, Prostaglandin J_2 and 15-deoxy-delta12,14-prostaglandin J_2 induce proliferation of cyclooxygenase-depleted colorectal cancer cells, Cancer Res. 59 (1999) 2739–2746.

[11] T. Hishinuma, Y. Koseki, Y. Murai, J. Kotake, F. Ishii, K. Suzuki, M. Mizugaki, Elevation of the thromboxane A_2/prostacyclin ratio in urine of diabetic mice analyzed by gas chromatography/selected ion monitoring, Prostaglandins 55 (1998) 83–93.

[12] T. Hishinuma, Y. Koseki, Y. Murai, T. Yamazaki, K. Suzuki, M. Mizugaki, Urinary thromboxane A_2/prostacyclin balance reflects the pathological state of a diabetic, Prostaglandins Other Lipid Mediat. 58 (1999) 263–271.

[13] T. Hishinuma, H. Tsukamoto, K. Suzuki, M. Mizugaki, Relationship between thromboxane/prostacyclin ratio and diabetic vascular complications, Prostaglandins Leukot Essent. Fatty Acids 65 (2001) 191–196.

[14] M. Nishikawa, T. Hishinuma, K. Nagata, Y. Koseki, K. Suzuki, M. Mizugaki, Effects of eicosapentaenoic acid (EPA) on prostacyclin production in diabetics: GC/MS analysis of PGI_2 and PGI_3 levels, Methods Find. Exp. Clin. Pharmacol. 19 (1997) 429–433.

[15] M. Cocozza, T. Picano, U. Oliviero, N. Russo, V. Coto, M. Milani, Effects of picotamide, an antithromboxane agent, on carotid atherosclerotic evolution. A two-year, double-blind, placebo-controlled study in diabetic patients, Stroke 26 (1995) 597–601.

[16] N. Suzuki, T. Hishinuma, F. Abe, K. Omata, S. Ito, M. Sugiyama, M. Mizugaki, Difference in urinary LTE4 and 11-dehydro-TXB_2 excretion in asthmatic patients, Prostaglandins Other Lipid Mediat. 62 (2000) 395–403.

[17] T. Hishinuma, H. Nakamura, T. Sawai, M. Uzuki, Y. Itabash, M. Mizugaki, Microdetermination of prostaglandin E_2 in joint fluid in rheumatoid arthritis patients using gas chromatography/selected ion monitoring, Prostaglandins Other Lipid Mediat. 58 (1999) 179–186.

[18] T. Hishinuma, Y. Koseki, J. Katayama, Y. Murai, T. Saito, M. Mizugaki, Changes of the thromboxane A2/prostacyclin balance in the urine of patients with renal diseases analyzed by gas chromatography/selected ion monitoring, Prostaglandins Other Lipid Mediat. 60 (2000) 1–8.

[19] H. Tsukamoto, T. Hishinuma, T. Mikkaichi, H. Nakamura, T. Yamazaki, Y. Tomioka, M. Mizugaki, Simultaneous quantification of prostaglandins, isoprostane and thromboxane in cell-culturted medium using gas chromatography-mass spectrometry, J. Chromatogr. B Analyt. Technol. Biomed. Life Sci. 774 (2002) 205–214.

[20] R. Baranowski, K. Pacha, Gas chromatographic determination of prostaglandins, Mini Rev. Med. Chem. 2 (2002) 135–144.

[21] D. Tsikas, Application of gas chromatography-mass spectrometry and gas chromatography-tandem mass spectrometry to assess in vivo synthesis of prostaglandins, thromboxane, leukotrienes, isoprostanes and related compounds in humans, J. Chromatogr. B Biomed. Sci. Appl. 717 (1998) 201–245.

[22] M. Takabatake, T. Hishinuma, N. Suzuki, S. Chiba, H. Tsukamoto, H. Nakamura, T. Saga, Y. Tomioka, A. Kurose, T. Sawai, M. Mizugaki, Simultaneous quantification of prostaglandins in human synovial cell-cultured medium using liquid chromatography/tandem mass spectrometry, Prostaglandins Leukot Essent. Fatty Acids 67 (2002) 51–56.

[23] R.C. Murphy, R.M. Barkley, B.K. Zemski, J. Hankin, K. Harrison, C. Johnson, J. Krank, A. McAnoy, C. Uhlson, S. Zarini, Electrospray ionization and tandem mass spectrometry of eicosanoids, Anal. Biochem. 346 (2005) 1–42.

[24] E. Brewer, J. Henion, Atmospheric pressure ionization LC/MS/MS techniques for drug disposition studies, J. Pharm. Sci. 87 (1998) 395–402.

[25] A. Margalit, K.L. Duffin, P.C. Isakson, Rapid quantitation of a large scope of eicosanoids in two models of inflammation: development of an electrospray and tandem mass spectrometry

method and application to biological studies, Anal. Biochem. 235 (1996) 73–81.
[26] C.S. Newby, A.I. Mallet, Rapid simultaneous analysis of prostaglandin E_2, 12-hydroxyeicosatetraenoic acid and arachidonic acid using high performance liquid chromatography/electrospray ionization mass spectrometry, Rapid Commun. Mass Spectrom. 11 (1997) 1723–1727.
[27] J.A. Hankin, P. Wheelan, R.C. Murphy, Identification of novel metabolites of prostaglandin E_2 formed by isolated rat hepatocytes, Arch. Biochem. Biophys. 340 (1997) 317–330.
[28] E.C. Kempen, P. Yang, E. Felix, T. Madden, R.A. Newman, Simultaneous quantification of arachidonic acid metabolites in cultured tumor cells using high-performance liquid chromatography/electrospray ionization tandem mass spectrometry, Anal. Biochem. 297 (2001) 183–190.
[29] K. Nithipatikom, N.D. Laabs, M.A. Isbell, W.B. Campbell, Liquid chromatographic-mass spectrometric determination of cyclooxygenase metabolites of arachidonic acid in cultured cells, J. Chromatogr. B Analyt. Technol. Biomed. Life Sci. 785 (2003) 135–145.
[30] Y. Kita, T. Takahashi, N. Uozumi, T. Shimizu, A multiplex quantitation method for eicosanoids and platelet-activating factor using column-switching reversed-phase liquid chromatography-tandem mass spectrometry, Anal. Biochem. 342 (2005) 134–143.
[31] R. Schmidt, O. Coste, G. Geisslinger, LC-MS/MS-analysis of prostaglandin E_2 and D_2 in microdialysis samples of rats, J. Chromatogr. B Analyt. Technol. Biomed. Life Sci. 826 (2005) 188–197.
[32] J. Kapron, J. Wu, T. Mauriala, P. Clark, R.W. Purves, K.P. Bateman, Simultaneous analysis of prostanoids using liquid chromatography/high-field asymmetric waveform ion mobility spectrometry/tandem mass spectrometry, Rapid Commun. Mass Spectrom. 20 (2006) 1504–1510.
[33] M. Mizugaki, T. Hishinuma, N. Suzuki, Determination of leukotriene E4 in human urine using liquid chromatography-tandem mass spectrometry, J. Chromatogr. B Biomed. Sci. Appl. 729 (1999) 279–285.
[34] Y. Murai, T. Hishinuma, N. Suzuki, J. Satoh, T. Toyota, M. Mizugaki, Determination of urinary 8-epi-prostaglandin F(2alpha) using liquid chromatography-tandem mass spectrometry: increased excretion in diabetics, Prostaglandins Other Lipid Mediat. 62 (2000) 173–181.
[35] N. Suzuki, T. Hishinuma, T. Saga, J. Sato, T. Toyota, J. Goto, M. Mizugaki, Determination of urinary 12(S)-hydroxyeicosatetraenoic acid by liquid chromatography-tandem mass spectrometry with column-switching technique: sex difference in healthy volunteers and patients with diabetes mellitus, J. Chromatogr. B Analyt. Technol. Biomed. Life Sci. 783 (2003) 383–389.
[36] N. Suzuki, T. Hishinuma, S. Chiba, T. Saga, H. Tsukamoto, M. Mizugaki, J. Goto, Quantitative liquid chromatography-tandem mass spectrometric analysis of 11-dehydro TXB_2 in urine, Prostaglandins Other Lipid Mediat. 73 (2004) 103–110.
[37] P. Yang, D. Chan, E. Felix, T. Madden, R.D. Klein, I. Shureiqi, X. Chen, A.J. Dannenberg, R.A. Newman, Determination of endogenous tissue inflammation profiles by LC/MS/MS: COX- and LOX-derived bioactive lipids, Prostaglandins Leukot Essent. Fatty Acids 75 (2006) 385–395.
[38] P. Araujo, L. Froyland, Optimisation of an extraction method for the determination of prostaglandin E_2 in plasma using experimental design and liquid chromatography tandem mass spectrometry, J. Chromatogr. B Analyt. Technol. Biomed. Life Sci. 830 (2006) 212–217.
[39] B.L. Diaz, H. Fujishima, Y. Kanaoka, Y. Urade, J.P. Arm, Regulation of prostaglandin endoperoxide synthase-2 and IL-6 expression in mouse bone marrow-derived mast cells by exogenous but not endogenous prostanoids, J. Immunol. 168 (2002) 1397–1404.
[40] I. Leal-Berumen, P. O'Byrne, A. Gupta, C.D. Richards, J.S. Marshall, Prostanoid enhancement of interleukin-6 production by rat peritoneal mast cells, J. Immunol. 154 (1995) 4759–4767.
[41] C. Feng, E.M. Beller, S. Bagga, J.A. Boyce, Human mast cells express multiple EP receptors for prostaglandin E_2 that differentially modulate activation responses, Blood 107 (2006) 3243–3250.
[42] S.G. Trivedi, J. Newson, R. Rajakariar, T.S. Jacques, R. Hannon, Y. Kanaoka, N. Eguchi, P. Colville-Nash, D.W. Gilroy, Essential role for hematopoietic prostaglandin D2 synthase in the control of delayed type hypersensitivity, Proc. Natl. Acad. Sci. USA 103 (2006) 5179–5184.
[43] K. Kabashima, D. Sakata, M. Nagamachi, Y. Miyachi, K. Inaba, S. Narumiya, Prostaglandin E_2-EP_4 signalling initiates skin immune responses by promoting migration and maturation of Langerhans cells, Nat. Med. 9 (2003) 744–749.
[44] G. Taguchi, Experimental Designs, Maruzen, Tokyo, 1962.
[45] L.J.II. Roberts, B.J. Sweetman, R.A. Lewis, K.F. Austen, J.A. Oates, Increased production of prostaglandin D_2 in patients with systemic mastocytosis, N. Engl. J. Med. 303 (1980) 1400–1404.
[46] J.A. Boyce, Eicosanoid mediators of mast cells: receptors, regulation of synthesis, and pathobiologic implications, Chem. Immunol. Allergy 87 (2005) 59–79.
[47] L.J.II. Roberts, R.A. Lewis, J.A. Oates, K.F. Austen, Prostaglandin thromboxane, and 12-hydroxy-5,8,10,14-eicosatetraenoic acid production by ionophore-stimulated rat serosal mast cells, Biochim. Biophys. Acta 575 (1979) 185–192.

doi: 10.1111/j.1365-3083.2007.02020.x

A Genetic Locus Controlling Aging-sensitive Regression of B Lymphopoiesis in an Autoimmune-prone MRL/lpr Strain of Mice

K. Nakatani*, W.-M. Qu†, M.-C. Zhang‡, H. Fujii†, H. Furukawa‡, T. Miyazaki†, M. Iwano*, Y. Saito*, M. Nose† & M. Ono‡

*First Department of Internal Medicine, Nara Medical University, Kashihara, Japan; †Department of Pathology, Ehime University School of Medicine, Toon, Japan; and ‡Department of Pathology, Tohoku University Graduate School of Medicine, Sendai, Japan

Received 20 June 2007; Accepted in revised form 14 August 2007

Correspondence to: M. Ono, Department of Pathology, Tohoku University Graduate School of Medicine, 2-1 Seiryo, Aoba-ku, Sendai, Miyagi 980-8575, Japan. E-mail: onomasao@mail.tains.tohoku.ac.jp

Abstract

Aging readily affects immune system under the influence of environmental and/or intrinsic factors while accelerating the development of various immune disorders including autoimmune diseases. Little is known about molecular and cellular mechanisms connecting between immune senescence and development of autoimmune diseases. Here, we first show strain-specific and aging-sensitive onset of B-cell abnormality in a lupus-prone MRL/Mp.Fas^{lpr} (MRL/lpr) strain of mice. This abnormality was characterized by the regression of B lymphopoiesis in the bone marrow of this strain. We next examined the association between the B-cell regression and onset of autoimmune diseases in aged (MRL/lpr × C3H/He.Fas^{lpr}) F_2 mice, in which pathologic phenotypes, such as glomerulonephritis, vasculitis, sialoadenitis and arthritis, variously developed. We also searched whole genome to identify genetic loci linked to the B-cell regression by using the same F_2 mice. The B-cell regression manifested in the spleen of F_2 mice was retrospectively evaluated by reverse transcriptase-based PCR quantification. The results demonstrated that the onset of autoimmune diseases in the F_2 mice was not associated with the aging-sensitive B-cell regression. The genetic study identified a significant locus responsible for the B-cell regression in the vicinity of *D5Mit233* (29 cM). This is first evidence for the presence of a genetic locus that affects B lymphopoiesis in an aging-sensitive manner.

Introduction

Homeostasis of immune system is essential for the integrity of our life. However, a state of immune homeostasis is thought to be changeable in response to intrinsic and environmental conditions. For example, aging as an intrinsic condition results in the regression of immune functions; a hygiene condition that influences an immune condition, i.e. a case of type 2 helper T-cell (Th2)-deviation presumably established under a modern hygiene condition and associated with human allergic disorders. It is a general understanding that a change in immune homeostasis has an impact on pathogenic mechanisms underlying various immune and infectious diseases. Aging is thought to be an important intrinsic factor for changing immune homeostasis, but little is known about an aging-sensitive homeostatic and pathogenic immune condition.

An animal experiment usually has the advantage of invariant genetic and environmental condition and provides an opportunity for longitudinal observation. An inbred strain of mice MRL/Mp.Fas^{lpr} (MRL/lpr) represents a model for human autoimmune diseases, which spontaneously develops lupus-like glomerulonephritis, systemic vasculitis, arthritis and sialadenitis [1–4]. An MRL/lpr strain carries a loss-of-function mutation of Fas gene (*lpr*) which encodes an apoptosis receptor on lymphocytes [5]. The *lpr* mutation is necessary for the onset of autoimmune diseases in MRL/lpr; however, the other *lpr*-congenic strains, including C3H/He.Fas^{lpr} (C3H/lpr), C57BL/6.Fas^{lpr} and AKR.Fas^{lpr}, barely develop autoimmune diseases [6–9]. The strain difference in the lpr constraint also influences the longevity of mice. An average age of death was estimated to be 17 weeks for female MRL/lpr, 22 weeks for male MRL/lpr and between 42 and 52 weeks for females on the C57BL/6J or C3H/HeJ

background (Mouse Genome Informatics, http://www.informatics.jax.org/menus/strain_menu.shtml). These facts indicate that the *lpr* mutation is not sufficient for the onset of autoimmune diseases, and that MRL/Mp-specific genetic conditions are prerequisite to the disease onset.

A number of studies have shown that Fas is essential for the prevention of autoreactive B-cell expansion [10–12]. In these studies, transgenic mouse models expressing autoantibody-encoding genes on B cells were studied when compared between Fas-deficient and Fas-sufficient strains. There is limited information on genetic background-specific autoimmune phenotype of B cells. To address this issue, we have used a non-autoimmune-prone C3H/lpr strain as well as a Fas-sufficient MRL/Mp (MRL/+) strain as reference strains for MRL/lpr. The combined use of these three strains enables us to evaluate effects of MRL/Mp-specific genetic factor and *lpr* on the onset of various autoimmune traits. Thereby, we have been attempting to identify strain-specific immune phenotypes and genetic polymorphisms associated with autoimmune diseases in MRL/lpr.

An autoimmune-prone strain of mice – BXSB – exhibits regression of B lymphopoiesis with aging [13]. This study proposed an aetiological link between this B-cell abnormality and autoimmune phenotypes in this strain. B cells expressing a single-antigen specificity to hen egg lysozyme (HEL) show spontaneous hyperactivity in the absence of self-antigen in MRL/lpr background [14]. Notably, this stain of mice was not only shown to have low total B-cell numbers but also an expansion of the marginal zone B-cell population. The proposed link remains to be shown in autoimmune strains of mice including MRL/lpr.

In the initial phase of the present study, we demonstrated a aging-dependent, significant decrease in the expression of FcγRIIb1 and CD22 in the spleen of MRL/lpr. FcγRIIb1 and CD22 are inhibitory receptors which physiologically regulate B-cell functions. A defect in either function of these receptors is known to entail autoimmune diseases in mice; therefore, their inhibitory functions are essential for the prevention of autoimmunity in B cells [15, 16]. Moreover, the genetic polymorphisms of these receptor genes have been suggested to be associated with autoimmune diseases in humans and mice [17–19]. The phenotype regarding FcγRIIb1 or CD22 is considered as a critical, causal impact on autoimmune diseases.

Genetic studies using autoimmune-prone strains of mice have revealed that the onset of most autoimmune traits is controlled by complex loci. Our previous studies using (MRL/lpr × C3H/lpr) (MC) F_2 mice identified differential sets of susceptibility loci controlling organ/tissue specificity of autoimmune disease [8], suggesting that background genes other than *lpr* determine tissue specificity of autoimmune disease. Here, we took advantage of accumulated data on the MCF_2 mice to evaluate an association between the B-cell regression and tissue-specific onset of autoimmune disease. Furthermore, we attempted to identify a responsible locus for the B-cell regression in the spleen by using the genome-wide microsatellite data of these mice. This study provides first evidence for the presence of genetic predisposition controlling B lymphopoiesis in an aging-sensitive manner.

Materials and methods

Mice. MRL/lpr and MRL/+ were purchased from Charles River Japan (Tokyo, Japan). C3H/lpr was purchased from The Jackson Laboratory (Bar Harbor, ME, USA). These mice were bred under specific pathogen-free conditions in the Integrated Center of Science, Ehime University, or the Animal Research Institute of Tohoku University Graduate School of Medicine. MCF_1 and MCF_2 mice were generated from female MRL/lpr and male C3H/lpr. In all animal experiments in this study, we observed the Tohoku University guideline or the Ehime University guideline for animal experimentation.

Flow cytometry. Spleen cells (10^6) were stained with the recommended dilution of fluorescence- or biotin-conjugated antibody in PBS containing 1% BSA on ice. All antibodies used in this study were purchased (BD PharMingen, San Diego, CA, USA). Streptavidin-conjugated allophycocyanin was used with a biotinylated antibody. We analysed small lymphocytic cells on the CellQuest software (Becton Dickinson, San Jose, CA, USA).

Reverse transcriptase-based PCR. Total RNA was isolated from spleen with ISOGEN (Nippon Gene, Tokyo, Japan). A first-strand cDNA was synthesized using random primer (Invitrogen, Carlsbad, CA, USA). Serially diluted cDNA products were subjected to reverse transcriptase-based PCR (RT-PCR) analyses. The transcripts were amplified by the following primers and conditions: FcγRIIb1/b2, AAGTCTAGGAAGGACACTGC and ATCCTGGCCTTTCTGGCTTGC, 28 cycles of 94 °C for 30 s, 55 °C for 30 s and 72 °C for 30 s; FcγRIIb1, AAGTCTAGGAAGGACACTGC and CCTCTGGAAGGGTTTCTCCCA, 20 cycles of 94 °C for 30 s, 55 °C for 30 s and 72 °C for 30 s; CD22, AAACTCCACTACCCAAGG and AGGTGATCTTAGAATCTTCC, 18 cycles of 94 °C for 30 s, 54 °C for 30 s and 72 °C for 30 s; CD19, AATCAGAGTCTAATCAACCAAG and GCCACCAGAGAAACCATACAGAAG by 18 cycles of 94 °C for 30 s, 55 °C for 30 s and 72 °C for 30 s; FcRγ, ATGATCTCAGCCGTGATCTTG and CTACTGGGGTGGTTTCTCATGCT, 22 cycles of 94 °C for 30 s, 55 °C for 30 s and 72 °C for 30 s; HPRT, GCTGGTGAAAAGGACCTCT and CACAGGACTAGAACACCTGC by 25 cycles of 94 °C for 30 s, 55 °C for 30 s and 72 °C for 30 s. PCR products were fractionated by electrophoresis in 2% agarose gel and were visualized after ethidium bromide staining.

A quantitative analysis was performed by real-time PCR system using the ABI Prism 7700 Sequence Detection System (Perkin-Elmer Applied Biosystems, Foster City, CA, USA). The FcγRIIb1 TaqMan™ probe (Perkin-Elmer Applied Biosystems) was CTATCTCAAGAAAAAGCAGGTTCCAGCTCTCCC. The forward and reverse primers for FcγRIIb1 amplification were GCAGCCATTGTTATTATCCTAGTATCC and CCTCTGGAAGGGTTTCTCCCA respectively. The CD22 TaqMan™ probe was TCCTCGGAGGCTGCGTGTGTCC. The forward and reverse primers for CD22 amplification were ATCGGAGAGACCTTGTCACAGG and ACTGTGAGATGGGCGGATTG respectively. The 18S rRNA TaqMan™ probe set was obtained from TaqMan™ Rodent 18S rRNA Control Reagents (Perkin-Elmer Applied Biosystems). The expression of FcγRIIb1, CD22 and 18S rRNA were quantified in separate tubes. We confirmed no amplification with the sample prepared in the absence of reverse transcriptase, indicating that a false signal originated from genomic DNA was negligible.

Histopathological examinations. All mice were killed under ether anesthesia at 16–20 weeks of age. We used histopathological grades determined previously for glomerulonephritis [20], arthritis [21–23], vasculitis [24, 25] and sialadenitis [26].

Microsattelite analysis and statistics. Genome-wide genotyping data of the MCF_2 mice determined in our previous study were used again in this study [26]. A hundred and six microsatellite markers cover whole autosomes with 12 cM apart with a maximum distance between any two markers of 37 cM. The positions of microsatellite loci were based on information from the Mouse Genome Database (MGD), The Jackson Laboratory (http://www.informatics.jax.org/menus/strain_menu.shtml). Association between genotype and expression index of FcγRIIb1 or CD22 was evaluated by an ANOVA. Significant and suggestive association was estimated based on a value of $P < 0.000052$ and $P < 0.0016$, respectively, as recommended by Lander and Kruglyak [27]. Quantitative trait locus (QTL) on chromosome 5 was determined with the data from 198 MCF_2 mice and the 11 microsatellite markers as indicated in Fig. 4. The mRNA expression levels of FcγRIIb1 and CD22 were $\log_{10}$ transformed. Logarithmic odds (LOD) scores were calculated by the interval mapping and the composite interval mapping methods in the Windows QTL Cartographer (Ver 2.5) software [28]. We adopted Model 6 with forward and backward regression methods for composite interval mapping. The number of control markers, the window size and the walk speed were set at 5, 10 cM and 2 cM respectively. A significant level was determined with the permutation test (1000 times) developed by Churchill and Doerge [29]. Difference of mean values of two groups was evaluated by the two-tailed multiple *t*-test with Bonferroni correction following an ANOVA.

Results

Aging-sensitive decrease in B-cell in the spleen of MRL/lpr mice

Comparing immune phenotypes between MRL/lpr and C3H/lpr, we eventually identified a marked change in the expression pattern of FcγRIIb1 and FcγRIIb2 in the spleen of 20-week-old MRL/lpr mice (Fig. 1A). The decrease was not observed in 8-week-old MRL/lpr mice. *FcγRIIB* gene is known to generate two alternative splicing products, FcγRIIb1 and FcγRIIb2. In spleen, FcγRIIb1 is expressed in B cells, while FcγRIIb2 is expressed in monocyte/macrophage and myeloid lineaged cells [30, 31]. Fig. 1A indicated a drastic conversion of FcγRIIb1/b2 ratio in the spleen of aged MRL/lpr mice, suggestive of a decrease in FcγRIIb1 expression, an increase in FcγRIIb2 expression or both. To address this concern, we examined relative protein amounts of FcγRIIb1 and FcγRIIb2 in the spleen by means of immunoprecipitation followed by Western blotting with FcγRIIb1/b2-specific antiserum. No evidence was obtained for relative increase in FcγRIIb2 protein expression (Fig. 1B), indicating that a decrease in FcγRIIb1 expression is a major event in the spleen of aged MRL/lpr mice.

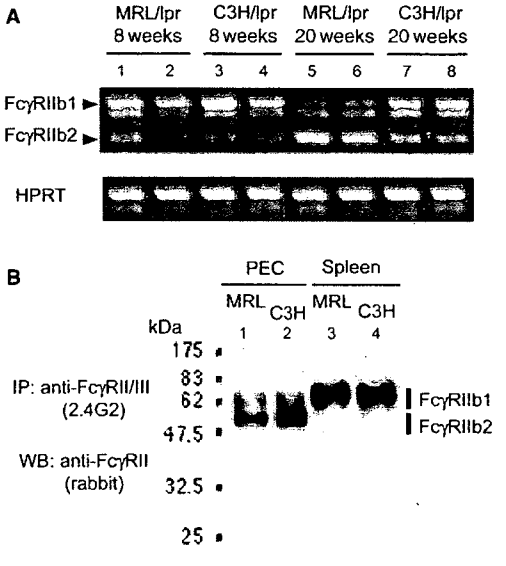

Figure 1 Expression of FcγRIIB isoforms (*FcγRIIb1 and FcγRIIb2*) in autoimmune-prone MRL/lpr and non-autoimmune-prone C3H/lpr mice. (A) RT-PCR assay showing aging-sensitive relative decrease in FcγRIIb1 expression in the spleen of aged (20-week-old) MRL/lpr mice. RT-PCR products obtained from two individual spleens were shown by ethidium bromide staining on an agarose gel. The comparable signal intensities of HPRT indicate equal loads of cDNA for all lanes. (B) Western blot analysis showing protein expression of FcγRIIB isoforms in the spleen and thioglycolate-induced peritoneal cells (PEC) in aged mice. MRL, aged MRL/lpr; C3H, aged C3H/lpr; IP, immunoprecipitation; WB, Western blot. Molecular weights (kDa) are indicated.

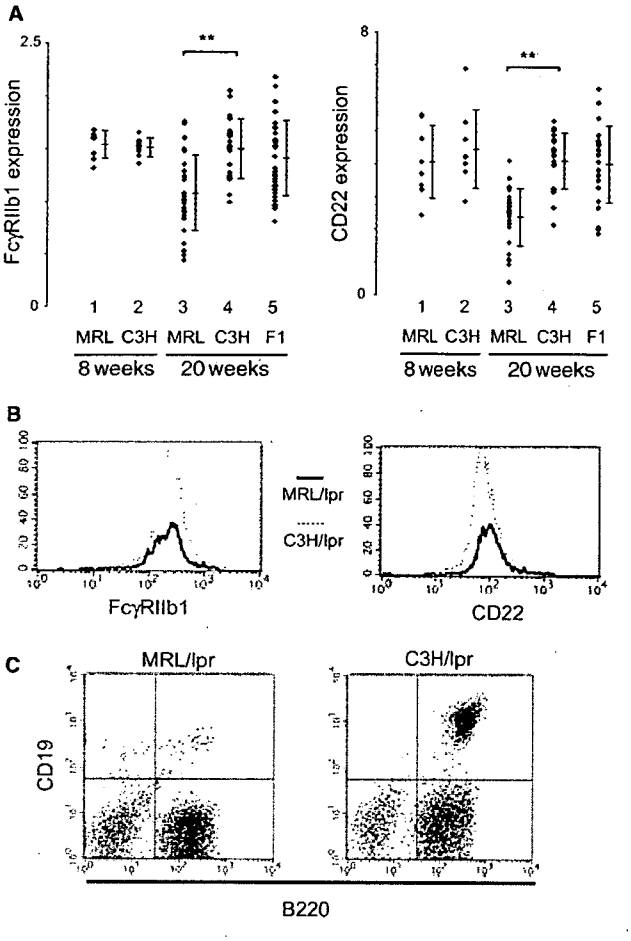

Figure 2 B-cell-related phenotypes in spleen. (A) RT-PCR quantification using the TaqMan™ probe showing significant decrease in FcγRIIb1 and CD22 expression in the spleen of an indicated strain of mice. Each bar represents the mean ± SD in each group. The difference of mean values of two groups was evaluated by the two-tailed multiple *t*-test with Bonferroni correction following one-way ANOVA. $^{**}P < 0.01$. (B) Flow cytometric analysis for B cells in the spleen of aged mice. B cells were gated as CD19-positive cells. The histogram showing a cell-surface expression level of FcγRIIb1 and CD22 protein. Three assays reproduced the same results. (C) Flow cytometric analysis using antibodies to CD45R (*B220*) and CD19 for the spleen cells of aged mice. Double-positive fraction includes B cells. CD45R (*B220*) single-positive cells are known to be *lpr*-T cells which uniquely appear in the Fas-deficient condition. This is a representative result summarized in Table 1 ($n = 4$).

Aging-sensitive and strain-dependent decrease in FcγRIIb1 expression in the spleen was confirmed for a large number of spleen samples by RT-PCR with FcγRIIb1-specific PCR primers (Fig. 2A). Another B-cell-specific molecule, CD22, represented an expression pattern similar to FcγRIIb1 (Fig. 2A). A flow cytometric analysis revealed comparable expression of FcγRIIb1 and CD22 protein on a single B cell (Fig. 2B). Importantly, spleen cell counts and a flow cytometric analysis with B-cell-specific markers, CD45R (denoted as B220 in the present figures) and CD19, confirmed a relative and absolute decrease in B-cell numbers in the spleen of aged MRL/lpr mice (Table 1, Fig. 2C). This tendency was observed in aged *Fas*-sufficient MRL/+ mice (Table 1).

Aging-sensitive decrease in B lymphopoiesis in MRL/lpr mice

A flow cytometric analysis using lineage markers for B-cell development revealed a remarkable decrease in B-cell precursors ($B220^+$ IgM^-), immature B cells ($B220^+$ IgM^+) and mature B cells ($B220^{high+}$ IgM^+) in the bone marrow of aged MRL/lpr (Table 1, Fig. 3A). This tendency was observed in aged MRL/+ mice (Table 1). RT-PCR assays consistently revealed a lower expression of B-cell-related transcripts, such as FcγRIIb1, CD22 and CD19, in the bone marrow of aged MRL/lpr mice, supporting the decrease in B lineage cells. On the other hand, Fc receptor gamma chain (FcRγ) was comparably detected for both strains (Fig. 3B). Overall findings indicate that the regression of B lymphopoiesis occurs in an aging-sensitive and MRL background-dependent fashion.

Association between the B-cell regression and onset of autoimmune diseases

We examined the association between the expression of B-cell-related transcripts, FcγRIIb1 and CD22, in the spleen and onset of autoimmune diseases in the MCF_2 mice. Statistically significant association was not observed with glomerulonephritis, renal vasculitis, sialadenitis or arthritis (Table 2).

A responsible locus for the B-cell regression

Using the genotype data of the MCF_2 mice determined previously [20, 26], we searched whole genome for genetic loci responsible for the B-cell regression in the MCF_2 mice. An MRL/lpr allele at *D5Mit233* (29 cM) was shown to be associated with a decrease in FcγRIIb1 expression in a recessive inheritance mode (Table 3). There was a clear tendency for an association between this locus genotype and CD22 expression in the same fashion; however, it was not statistically supported (Table 3). The interval and composite interval mapping of a QTL analysis demonstrated a single LOD peak at 26 cM and 24 cM for FcγRIIb1 and CD22 traits respectively (Fig. 4). Threshold levels of LOD with statistical significance were estimated to be 3.24 ($\alpha = 0.01$) and 2.26 ($\alpha = 0.05$) for FcγRIIb1 loci and 3.01 ($\alpha = 0.01$) and 2.25 ($\alpha = 0.05$) for CD22 loci by the permutation test.

Discussion

The present study provided first evidence for aging-dependent regression of B lymphopoiesis in an

Table 1 The number or fraction of B lineage cells in the spleen and bone marrow of aged MRL and C3H mice.

	Genotype	Unit	Strain of mice MRL	C3H	Statistics[a]
Spleen					
Total cell counts	*lpr/lpr*	$\times 10^6$	278 (63.1)	260 (26.9)	
	+/+	$\times 10^6$	37.5 (8.70)	45.3 (8.54)	
B cells ($B220^+$ $CD19^+$)	*lpr/lpr*	$\times 10^6$	20.9 (15.9)	87.7 (18.4)	**
	+/+	$\times 10^6$	8.43 (1.54)	14.9 (1.96)	**
Bone marrow					
B precursors (IgM^-B220^+)	*lpr/lpr*	%	10.9 (2.82)	26.6 (3.54)	**
	+/+	%	6.25 (1.17)	14.4 (2.16)	**
Immature B (IgM^+B220^+)	*lpr/lpr*	%	3.48 (1.23)	5.75 (0.57)	*
	+/+	%	2.60 (0.67)	4.43 (0.53)	**
Mature B (IgM^+B220^{++})	*lpr/lpr*	%	1.55 (0.87)	6.65 (1.30)	**
	+/+	%	4.98 (1.58)	8.08 (1.30)	*

[a]Two-tailed *t*-test: $^{**}P < 0.01$; $^{*}P < 0.05$.
Each value represents the mean (SD) of four mice.

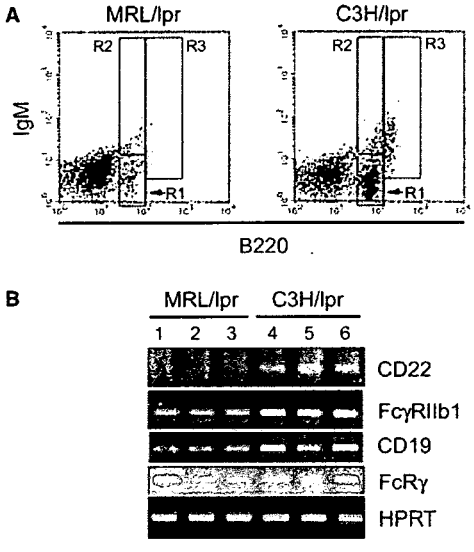

Figure 3 B-cell-related phenotypes in bone marrow. (A) Flow cytometric analysis using antibodies to CD45R (*B220*) and IgM showing the development of B cells in the bone marrow cells of aged mice. Indicated boxes in the dot-gram include pro- and pre-B cells (*R1*), immature B cells (*R2*) and mature B cells (*R3*). This is a representative result summarized in Table 1 ($n = 4$). (B) RT-PCR assay showing relative decrease in B-cell-related transcripts (*CD22*, *FcγRIIb1* and *CD19*) in the bone marrow of aged (20-week-old) MRL/lpr mice. RT-PCR products obtained from three individual spleens were shown by ethidium bromide staining on agarose gels. The comparable signal intensities of HPRT indicate equal loads of cDNA for all lanes.

MRL/lpr lupus strain and genetic regulation of this phenotype. It is of particular note that this phenotype depends on strain-specific genetic background but not on the *lpr* mutation. The significance of genetic background has been emphasized in the lpr-dependent autoimmunity. It has been explored how the genetic background alters immune phenotypes toward autoimmune diseases in an MRL/lpr strain. If such phenotype was found, it would be accounted as a cellular target for autoimmune therapy. In the initial phase of this study, we found a remarkable, strain-specific, *lpr*-independent decrease in peripheral B-cell number in MRL/lpr mice. These findings facilitated us to investigate the correlation between the B-cell regression and autoimmune onset. The MCF_2 mice, which were previously generated to identify QTL of autoimmune diseases, provided us with an opportunity for the evaluation of the correlation. The results rather indicate that the B-cell regression in MRL/lpr mice is not a cause of autoimmune disease. This conclusion is also supported by the genetic findings that the present locus located near *D5Mit233* does not overlap with any of autoimmune loci previously identified in associations with glomerulonephritis [20], arthritis [21–23], vasculitis [24, 25] and sialadenitis [26]. We failed to show the significant association of this phenotype with the onset of glomerulonephritis, ranal arthritis, vasculitis and sialadenitis. Other autoimmune phenotypes such as pancreatitis and a series of autoantibody production should be investigated. It is also an interesting question whether the B-cell regression of interest influences susceptibility to vaccinated antigen or infection.

Hypergamma globulinemia is generally characteristic of autoimmune disease. MRL/lpr mice readily exhibit this trait with aging and disease onset. The decline of B-cell numbers in the spleen and bone marrow with aging in MRL/lpr seems to conflict with prominent hypergamma globulinemia in this strain. Similar to the MRL/lpr case, a remarkable decrease in B lymphopoiesis with aging was demonstrated in another autoimmune-prone BXSB strain of mice [13]. Another study has shown that B cells expressing single-antigen specificity to HEL represent spontaneous hyperactivity in the absence of self-antigen in MRL/lpr background. Notably, this stain of mice was not only shown to have low total B-cell

Table 2 Association of FcγRIIbl or CD22 expression with the autoimmune trait manifested in MCF_2 mice.

	FcγRIIbl			CD22		
	Onset of disease[a]			Onset of disease[a]		
	+	−	P^b	+	−	P^b
Glomerulonephritis	0.96 (0.42)	0.97 (0.39)	0.883	2.49 (0.92)	2.71 (1.22)	0.213
Renal vasculitis	0.98 (0.39)	0.97 (0.40)	0.905	2.68 (1.14)	2.66 (1.16)	0.935
Arthritis	1.00 (0.40)	0.97 (0.40)	0.696	2.66 (1.17)	2.66 (1.16)	0.990
Sialadenitis	0.98 (0.37)	0.96 (0.41)	0.825	2.63 (1.12)	2.67 (1.22)	0.769

[a]Onset of each disease was defined in the previous reports (see *Materials and methods*). +, diseased; −, not affected.
[b]Two-tailed *t*-test.
Each value represents the mean (SD) of FcγRIIbl or CD22 expression index.

Table 3 Association of FcγRIIbl and CD22 expression with microsatellite genotypes on chromosome 5.

		Genotype			
Marker	cM	*MM*[a]	*MC*[a]	*cc*[a]	P^b
FcγRIIbl expression					
D5Mit145	0	0.86 (0.34)	0.98 (0.41)	1.07 (0.40)	0.025
D5Mit74	11	0.84 (0.34)	1.00 (0.42)	1.05 (0.38)	0.0037
D5Mit149	19	0.80 (0.34)	1.02 (0.42)	1.03 (0.37)	0.00085[c]
D5Mit233	29	0.80 (0.28)	1.04 (0.46)	1.02 (0.33)	0.00015[c]
D5Mit134	41	0.83 (0.28)	1.01 (0.46)	1.05 (0.33)	0.0025
D5Mit115	56	0.86 (0.30)	1.01 (0.47)	1.01 (0.31)	0.0270
CD22 expression					
D5Mit145	0	2.31 (0.90)	2.68 (1.13)	2.95 (1.35)	0.017
D5Mit74	11	2.30 (0.97)	2.73 (1.12)	2.92 (1.32)	0.0076
D5Mit149	19	2.23 (0.97)	2.77 (1.12)	2.84 (1.27)	0.0046
D5Mit233	29	2.25 (1.04)	2.81 (1.10)	2.80 (1.28)	0.0053
D5Mit134	41	2.40 (1.12)	2.64 (1.10)	2.93 (1.25)	0.054
D5Mit115	56	2.41 (1.10)	2.69 (1.13)	2.86 (1.24)	0.092

[a]*MM*, *MC* and *CC* represent the genotypes at indicated marker positions: MRL/MRL homozygote, MRL/C3H heterozygote and C3H/C3H homozygote respectively.
[b]One-way layout ANOVA.
[c]Suggestive linkage.
Each value represents the mean (SD) in each genotype group.

numbers but also an expansion of the marginal zone B-cell population. These findings may lead to a new insight revealing general correlation between B-cell regression and autoimmune onset.

Here, we demonstrated the regression of B lymphopoiesis in not only autoimmune MRL/lpr mice but also non-autoimmune MRL/+ mice. This finding suggests that the B-cell regression is not an effect of autoimmunity. Functional B cells are established after undergoing multiple differentiation stages in bone marrow and peripheral lymphoid tissues. Aging has been shown to spontaneously, readily impair B lymphopoiesis [32–34]. A molecular mechanism of the impact of aging on B lymphopoiesis remains unclear. The genetic information obtained from this study provides a clue to clarify this issue.

The locus identified in this study includes candidate genes that function with immunological importance. This locus is syntenic of human chromosome interval between 4p14 and 4p16.3. Considering gene functions for B-cell activation and differentiation, we presently evaluate *Bst1* (bone marrow stromal cell antigen 1, 25 cM) and *Cd38* (CD38, 28 cM) as the positional candidates. The two genes encode a similar type of cell surface receptors belonging to the super family of ADP-ribosyl cyclase. *Bst1* product is present on bone marrow stromal cells which regulate B lymphopoiesis [35]. *Cd38* product is present on B lineage cells and serve as a receptor which mediates the signal for the suppression of B lymphopoiesis [36, 37] and the modulation of B-cell functions [38, 39]. Polymorphic nature of these molecules is of primary interest as concerning the B-cell regression manifested in MRL/lpr mice.